SKB

TECHNICAL REPORT 94-21

Verification of HYDRASTAR: Analysis of hydraulic conductivity fields and dispersion

S T Morris, K A Cliffe

AEA Technology, Harwell, UK

October 1994

SVENSK KÄRNBRÄNSLEHANTERING AB
SWEDISH NUCLEAR FUEL AND WASTE MANAGEMENT CO
BOX 5864 S-102 40 STOCKHOLM
TEL. 08-665 28 00 TELEX 13108 SKB S
TELEFAX 08-661 57 19

VERIFICATION OF HYDRASTAR: ANALYSIS OF HYDRAULIC CONDUCTIVITY FIELDS AND DISPERSION

S T Morris, K A Cliffe

AEA Technology, Harwell, UK

October 1994

Verification of HYDRASTAR: Analysis of Hydraulic Conductivity Fields and Dispersion

S T Morris and K A Cliffe

AEA Technology
424.4 Harwell
Didcot
Oxon OX11 0RA

October 1994

Verification of HYDRASTAR: Analysis of Hydraulic Conductivity Fields and Dispersion

S T Morris and K A Cliffe

Abstract (English)

HYDRASTAR is a code for the stochastic simulation of groundwater flow. It can be used to simulate both time-dependent and steady-state groundwater flow at constant density. Realizations of the hydraulic conductivity field are generated using the Turning Bands algorithm. The realizations can be conditioned on measured values of the hydraulic conductivity using Kriging. This report describes a series of verification studies that have been carried out on the code. The first study concerns the accuracy of the implementation of the Turning Bands algorithm in HYDRASTAR. The implementation has been examined by evaluating the ensemble mean and covariance of the generated fields analytically and comparing them with their prescribed values. Three other studies were carried out in which HYDRASTAR was used to solve problems of uniform mean flow and to calculate the transport and dispersion of fluid particles. In all three cases the hydraulic conductivity fields were unconditioned. The first two were two-dimensional: one at small values of the variance of the logarithm of the hydraulic conductivity for which there exists analytical results that the code can be compared with, and one at moderate variance where the results can only be compared with those obtained by another code. The third problem was three dimensional with a small variance and again analytical results are available for comparison.

Keywords: stochastic simulation, groundwater flow, hydraulic conductivity, Turning Bands algorithm, dispersion, transport, verification.

Verification of HYDRASTAR: Analysis of Hydraulic Conductivity Fields and Dispersion

S T Morris and K A Cliffe

Abstract (Swedish)

HYDRASTAR är en kod för stokastisk simulering av grundvattenströmning. Simulering görs under antagande om konstant densitet för grundvattnet. Transienta problem kan även studeras. Den s k Turning Bands-algoritmen används för generering av realiseringar av fältet för hydraulisk konduktivitet. Dessa realiseringar kan betingas med kriging mot uppmätta konduktivitetsvärden.

Denna rapport beskriver en serie av verifieringsövningar som utförts med programkoden. Den första delen berör noggrannheten av implementeringen av Turning Bands-algoritmen. Medelvärden och kovarians för fälten har utvärderats analytiskt och jämförts med föreskrivna värden. De tre övriga fallen behandlar advektiv transport och dispersion i HYDRASTAR för ett homogent flödesfält. I alla tre fallen rör det sig om obetingad simulering. Det två första är 2D-exempel: ett med ett litet värde för variansen på log-K för vilket det existerar analytiska lösningar, ett med måttlig varians där resultaten kan jämföras med en annan programkod. Det tredje och sista exemplet är i 3D, åter igen med liten varians eftersom analytiska lösningar finns tillgängliga för detta fall.

EXECUTIVE SUMMARY

HYDRASTAR is a code for the stochastic simulation of groundwater flow. The current version, 1.4, solves either time-dependent or steady state groundwater flow with constant density in three dimensions. The governing partial differential equations are discretized by a finite-difference method. A pre-conditioned conjugate-gradient algorithm is used to solve the discretized equations. Realizations of the hydraulic conductivity field are generated using the Turning Bands algorithm. These realizations can be conditioned on measured values of the hydraulic conductivity using Kriging. Transport is treated by a purely advective algorithm.

The purpose of this report is to describe a set of verification tests carried out on the code. The tests have been carefully designed to complement and extend the verification work already carried out by Norman. Four verification studies have been carried out.

The first is an analytical study of the performance of the implementation of the Turning Bands algorithm used to generate realizations of the hydraulic conductivity fields. A number of potential defects of hydraulic conductivity fields generated by the Turning Bands algorithm have been identified in the literature. These defects usually show themselves as additional, unwanted, spatial structures often called striping. The problem is particularly acute in three dimensions where it is much harder to get a satisfactory distribution of the Bands in space. The approach adopted in the present study is to take the method used in HYDRASTAR and to evaluate the mean and covariance of the generated fields analytically. The expressions derived in this way apply to the ensemble statistics. This approach complements that of Norman, who calculated the one-dimensional and multi-dimensional variograms from a finite number of realizations. The expressions obtained for the mean and covariance are quite complicated. Nevertheless they make it possible to determine the cause of the striping and to assess to what extent modifying the parameters used in the algorithm will overcome the problems. The results indicate that, with the values of the parameters recommended by Norman, the mean, variance and covariance of the generated fields, with either exponential or spherical covariance, are sufficiently accurate for most practical purposes. There is some evidence of striping but the effect is small and the maximum error in the covariance in any direction, due to the finite number of lines, is approximately 10% of the variance. The maximum error of the covariance averaged over all directions is just 3% of the variance.

In the second study the case of uniform mean flow at small variance of the logarithm of hydraulic conductivity was considered. There is an analytical solution

for the first and second order moments of velocity and for the particle displacements in this case. Calculations carried out using HYDRASTAR to solve this problem were compared with the analytic results. The agreement was found to be satisfactory. In particular, the moments of particle displacement are in very good agreement with those obtained by Dagan. Since this type of calculation uses most of the numerical and statistical functions of the code, this test indicates that HYDRASTAR is capable of calculating accurately both the flow and transport in two-dimensional flows with small variance of the logarithm of hydraulic conductivity.

The third study concerns the same problem as the second mentioned above, except that the variance is no longer small. In this case there is no valid analytical solution and so the results obtained with HYDRASTAR were compared with the two-dimensional code SPV2D, developed by AEA Technology. The results of HYDRASTAR and SPV2D were found to be reasonably consistent. However, a number of numerical difficulties were encountered. Firstly, the numerical errors are larger, due to the larger variance. It is possible to reduce these errors by refining the computational mesh, but the errors reduce very slowly as the mesh size is increased. In fact, the error in the velocity is only halved as the mesh spacing is reduced by a factor of 4. Hence, the mesh refinement needs to be significantly greater than in the case of small variance. Secondly, because the dispersion is greater, a larger computational domain is required. Thirdly, many more iterations are needed to solve the flow equation. The condition number of the matrices arising from the discretisation increases as the variance increases. Since the rate of convergence of the PCCG method decreases with increasing condition number this is not unexpected. Finally, because of the increased variability of the solution, more realizations are needed to obtain equally reliable statistics. The combined effect of all these factors is that significantly more computation time is needed for the runs with moderate variance, compared to those at small variance. Thus one conclusion of this part of the study is that it is difficult to obtain accurate results in the case of moderate or large variance and the computational cost of doing so may be very high with the methods used in HYDRASTAR.

The final part of this study concerns the case of uniform flow in three dimensions at small variance. As in the two-dimensional case there is an analytic solution for the second order moments of the particle displacements. Calculations carried out using HYDRASTAR to solve this problem were compared with the analytic results. The agreement was found to be satisfactory. In particular, the moments of particle displacement are in good agreement with those obtained by Dagan. Again this indicates that HYDRASTAR is capable of calculating accurately both the flow and transport in three-dimensional flows with small variance of the logarithm of hydraulic conductivity.

These studies complement and extend the results obtained by Norman, and help to build confidence that the code will produce correct results when applied to realistic cases.

CONTENTS

TABLES

FIGURES

1. INTRODUCTION

HYDRASTAR [1], [2] is a code for the stochastic simulation of groundwater flow. The current version, 1.4, solves either time-dependent or steady state groundwater flow with constant density in three dimensions. The governing partial differential equations are discretized by a finite-difference method. A pre-conditioned conjugate-gradient algorithm is used to solve the discretized equations. Realizations of the hydraulic conductivity field are generated using the Turning Bands algorithm. These realizations can be conditioned on measured values of the hydraulic conductivity using Kriging. Transport is treated by a purely advective algorithm.

The code has recently been used to model the Finnsjön site, as part of the SKB-91 Project. This is one of the first stochastic continuum studies to be carried out for a real site in three dimensions. The success of the study demonstrates that HYDRASTAR is one of the world's leading stochastic continuum programs.

The purpose of this report is to describe a set of verification tests carried out on the code. The tests have been carefully designed to complement and extend the verification work already carried out by Norman [3]. Norman produced results from HYDRASTAR for two example problems. The first concerned the flow in a three-dimensional unconditioned random hydraulic conductivity field with small variance. In this case it is possible to solve for the groundwater head analytically. Norman compared the results for the semivariogram of the hydraulic head produced by HYDRASTAR with the analytic solution. Generally satisfactory agreement was found but with some shortcomings, due to limitations on the mesh refinement that could be used. The second case that Norman examined was HYDROCOIN [4] case 2. This is a purely deterministic example whose principal feature is the presence of several narrow fracture zones with high hydraulic conductivity. The results obtained with HYDRASTAR were in good agreement with those obtained in the HYDROCOIN project.

Two types of verification study have been carried out in the work reported here. The first is an analytical study of the performance of the implementation of the Turning Bands algorithm used to generate realizations of the hydraulic conductivity fields. A number of potential defects of hydraulic conductivity fields generated by the Turning Bands algorithm have been identified in the literature [5], [6]. These defects usually show themselves as additional, unwanted, spatial structures often called striping. The problem is particularly acute in three dimensions where it is much harder to get a satisfactory distribution of the Bands in space. The approach adopted in the present study is to take the method used in HYDRASTAR and to

evaluate the mean and covariance of the generated fields analytically. The expressions derived in this way apply to the ensemble statistics. This approach complements that of Norman, who calculated the one-dimensional and multi-dimensional variograms from a finite number of realizations. The expressions obtained are quite complicated. Nevertheless they make it possible to determine the origin of the striping and to assess to what extent modifying the parameters used in the algorithm overcome the problems. The method used and the results obtained are described in detail in Section 2.

In the second type of verification study several flow problems have been examined in order to assess how accurately HYDRASTAR calculates the transport in the stochastic flow fields. It is very important to examine and verify HYDRASTAR for this type of calculation since in a performance assessment for a potential radioactive waste repository it is the transport characteristics of the site that are of crucial importance. Thus the test cases that have been set up and studied extend the work done by Norman on his first example [3].

Three problems have been studied. All have hydraulic conductivity fields with a constant mean and hydraulic head boundary conditions which would support a uniform flow solution in the case of a constant hydraulic conductivity. The first two cases are two-dimensional. In the case described in Section 3 the variance of the hydraulic conductivity field is taken to be small and in this case the problem has an analytical solution for the longitudinal and transverse dispersion of particle paths, first obtained by Dagan [7]. The results obtained by HYDRASTAR are compared with the analytical results of Dagan.

In Section 4 the problem studied in Section 3 is repeated at a moderate value of the variance. In this case the results of Dagan are not guaranteed to be accurate and so the results obtained with HYDRASTAR are compared with those obtained with the program SPV2D, which was written by AEA Technology. SPV2D is much more limited in its scope than HYDRASTAR and was specifically written to study dispersion in heterogeneous media at moderate and large variances. It is clearly not as satisfactory to compare the results of HYDRASTAR with those of another code as it is to compare them with exact analytical results. However, it is quite possible that HYDRASTAR will have to be used in practice to study cases with moderate or even large variance and so this exercise is well worth doing.

Finally, in Section 5, a three-dimensional problem with small variance is studied. This, again, has an analytical solution with which the results of HYDRASTAR can be compared.

The HYDRASTAR input datasets used in this study are included in the appendices.

2. GENERATION OF HYDRAULIC CONDUCTIVITY FIELDS

2.1 The Turning Bands Algorithm

The Turning Bands Algorithm (TBA) is used by HYDRASTAR to generate realizations of the random hydraulic conductivity field. The hydraulic conductivity K is obtained by an exponential transform of a real Gaussian random field, Y, using the relation

$$K(\mathbf{x}) = K_0 e^{Y(\mathbf{x})}, \tag{1}$$

where K_0 is the geometric mean of the hydraulic conductivity. The hydraulic conductivity values are therefore log-normally distributed.

In this Section, we derive analytic expressions for the ensemble mean, variance and covariance of the fields generated by the Turning Bands Algorithm as implemented in HYDRASTAR. The dependence of these statistics on the parameters used are evaluated, and these results are used to estimate the size of the errors expected from the choice of parameters used by HYDRASTAR.

The TBA generates realizations of a real Gaussian spatial process, $Y(\mathbf{x})$. The field is completely defined by its mean

$$\mu(\mathbf{x}) = E[Y(\mathbf{x})], \tag{2}$$

and covariance

$$C(\mathbf{x}_1, \mathbf{x}_2) = E[(Y(\mathbf{x}_1) - \mu(\mathbf{x}_1))(Y(\mathbf{x}_2) - \mu(\mathbf{x}_2))], \tag{3}$$

where $E[...]$ denotes expectation.

The field is second-order stationary. That is, the first two moments are invariant under translation

$$\mu(\mathbf{x}) = \mu, \tag{4}$$

$$C(\mathbf{x}_1, \mathbf{x}_2) = C(\mathbf{h}), \tag{5}$$

where $\mathbf{h} = \mathbf{x}_1 - \mathbf{x}_2$.

The principle of the method is to generate a three-dimensional field by superposition of one-dimensional fields generated along lines radiating from the origin. Consider Figure 2.1. Let there be N lines with direction vectors $\mathbf{l}_i$. The field value generated at a point $\mathbf{x}$ is

$$Y_S(\mathbf{x}) = \frac{1}{\sqrt{N}} \sum_{i=1}^{N} Y_i((\mathbf{x}.\mathbf{l}_i), \mathbf{l}_i), \tag{6}$$

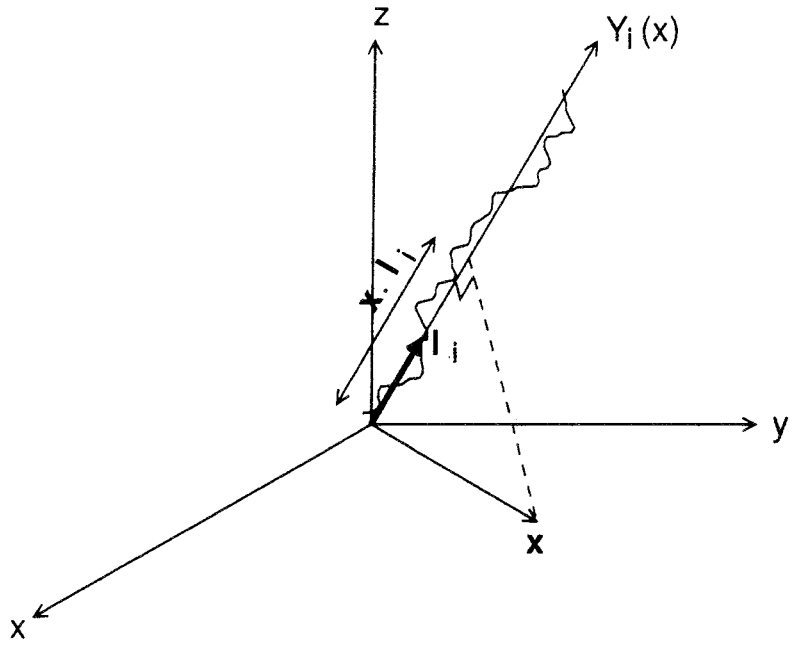

Figure 2.1: Turning Bands geometry showing the ith line and a field point $\mathbf{x}$.

where $Y_i((\mathbf{x}.\mathbf{l}_i), \mathbf{l}_i)$ is an independent one-dimensional second-order stationary random function. In practice the one-dimensional process $Y_i((\mathbf{x}.\mathbf{l}_i), \mathbf{l}_i)$ is generated discretely at points with separation b. The discretization of the lines defines a set of planes, or bands, perpendicular to the lines in space. On each line in turn the orientation of the bands is different. This is the origin of the name 'Turning Bands'.

The one-dimensional random process may be generated in a number of different ways [8], [5], [9]. HYDRASTAR uses the 'moving average' method [8]. This is based on the observation that any one-dimensional covariance function can be expressed as a convolution integral. Norman [3] derives approximate expressions for the generation of one-dimensional random processes using the moving-average method, for spherical and exponential covariance models.

The spherical covariance model is defined by

$$C(r) = \begin{cases} V\left(1 - \frac{3}{2}\frac{r}{a} + \frac{1}{2}\frac{r^3}{a^3}\right) & 0 \leq r \leq a, \\ 0 & a < r, \end{cases} \tag{7}$$

and the exponential covariance model by

$$C(r) = Ve^{-\lambda r}, r \geq 0, \tag{8}$$

where V is the variance, r the separation between points, and a and λ are range parameters.

The expressions used by HYDRASTAR to generate these line processes are,

for the spherical case

$$Y_i(jb) = \sqrt{\frac{3V}{\sigma_t^2(2R^3+3R^2+R)}} \sum_{k=-R}^{R} k t_{k-j}, \tag{9}$$

and for the exponential case

$$Y_i(jb) = \sqrt{\frac{V}{\sigma_t^2 \Sigma}} \sum_{k=0}^{8R} \left(1 - \lambda\left(k+\frac{1}{2}\right)b\right) e^{-\lambda k b} t_{k-j}, \tag{10}$$

where

$$\Sigma = \sum_{k=0}^{8R} \left(1 - \lambda b\left(k+\frac{1}{2}\right)\right)^2 e^{-2\lambda k b}, \tag{11}$$

R is an integer parameter, the parameter b is determined from the requirement that $a = (2R+1)b$ in the spherical case, and $(8R+1)b = 4\lambda$ in the exponential case, and t_k are independent random variables with moments

$$E[t_k] = 0, \tag{12}$$

and

$$E[{t_k}^2] = \sigma_t^2, \tag{13}$$

j is determined by the projection of $\mathbf{x}$ onto $\mathbf{l}_i$, such that

$$(j-1)b \leq \mathbf{x}.\mathbf{l}_i < jb. \tag{14}$$

From equation (6), the field value generated at position $\mathbf{x}$ using these expressions is, in the case of a spherical covariance

$$Y_S(\mathbf{x}) = \frac{1}{\sqrt{N}} \sqrt{\frac{3V}{\sigma_t^2(2R^3+3R^2+R)}} \sum_{i=1}^{N} \sum_{k=-R}^{R} k t_{k-j}, \tag{15}$$

and for an exponential covariance

$$Y_S(\mathbf{x}) = \frac{1}{\sqrt{N}} \sqrt{\frac{V}{\sigma_t^2 \Sigma}} \sum_{i=1}^{N} \sum_{k=0}^{8R} (1 - \lambda(k+\frac{1}{2})b) e^{-\lambda k b} t_{k-j}. \tag{16}$$

2.2 The Mean

It follows from equations (15) and (16), together with the fact that $E[t_k] = 0$ that the expectation of the field generated by the TBA, as used in HYDRASTAR, is zero everywhere, independent of the choice of parameters R, N, and of the directions $\mathbf{l}_i$ of the Turning Bands lines.

2.3 The Covariance and Variance

The covariance of the generated field for a pair of points $\mathbf{x}$, $\mathbf{x}'$ is

$$\begin{aligned} C_S(\mathbf{x},\mathbf{x}') &= E[Y_S(\mathbf{x})Y_S(\mathbf{x}')], \\ &= E\left[\frac{1}{\sqrt{N}}\sum_{i=1}^{N} Y_i((\mathbf{x}.\mathbf{l}_i),\mathbf{l}_i)\frac{1}{\sqrt{N}}\sum_{i'=1}^{N} Y_{i'}((\mathbf{x}'.\mathbf{l}_{i'}),\mathbf{l}_{i'})\right], \\ &= \frac{1}{N}\sum_{i=1}^{N}\sum_{i'=1}^{N} E\left[Y_i((\mathbf{x}.\mathbf{l}_i),\mathbf{l}_i)Y_{i'}((\mathbf{x}'.\mathbf{l}_{i'}),\mathbf{l}_{i'})\right]. \end{aligned} \tag{17}$$

In the case of a spherical covariance, from (15) this expression becomes

$$C_S(\mathbf{x},\mathbf{x}') = \frac{1}{N}\frac{3V}{\sigma_t^2(2R^3+3R^2+R)}\sum_{i=1}^{N}\sum_{i'=1}^{N}\sum_{k=-R}^{R}\sum_{k'=-R}^{R} E[kk't_{k-j}t_{k'-j'}]. \tag{18}$$

Now, if $i \neq i'$, then t_{k-j} and $t_{k'-j'}$ are independent, and hence $E[kk't_{k-j}t_{k'-j'}] = 0$. Therefore

$$C_S(\mathbf{x},\mathbf{x}') = \frac{1}{N}\frac{3V}{\sigma_t^2(2R^3+3R^2+R)}\sum_{i=1}^{N}\sum_{k=-R}^{R}\sum_{k'=-R}^{R} E[kk't_{k-j}t_{k'-j'}]. \tag{19}$$

Consider $\omega = \sum_{k=-R}^{R}\sum_{k'=-R}^{R} E[kk't_{k-j}t_{k'-j'}]$. Let $m = k - j$ and let $m' = k' - j'$. Then

$$\omega = \sum_{m=-R-j}^{R-j}\sum_{m'=-R-j'}^{R-j'} E[(m+j)(m'+j')t_m t'_m], \tag{20}$$

$$E[t_m t'_m] = \begin{cases} \sigma_t^2 & \text{if } m = m', \\ 0 & \text{if } m \neq m'. \end{cases} \tag{21}$$

Hence

$$\omega = \sum_{m=MAX(-R-j,-R-j')}^{MIN(R-j,R-j')} \sigma_t^2(m+j)(m+j'). \tag{22}$$

Therefore

$$C_S(\mathbf{x},\mathbf{x}') = \frac{1}{N}\frac{3V}{(2R^3+3R^2+R)}\sum_{i=1}^{N}\sum_{m=MAX(-R-j,-R-j')}^{MIN(R-j,R-j')} (m+j)(m+j'). \tag{23}$$

Equation (23) gives the covariance of the ensemble of realizations of a field with a prescribed spherical covariance, generated by the TBA as implemented in HYDRASTAR. The equation is valid for any values of the parameters R, N, and of the directions $\mathbf{l}_i$ of the Turning Bands lines.

A special case arises when $\mathbf{x} = \mathbf{x}'$. In this case, $j = j'$, and

$$\begin{aligned} Var(\mathbf{x}) &= \frac{1}{N}\frac{3V}{(2R^3+3R^2+R)}\sum_{i=1}^{N}\sum_{m=-R-j}^{R-j}(m+j)^2, \\ &= \frac{3V}{(2R^3+3R^2+R)}\sum_{k=-R}^{R}k^2, \\ &= V. \end{aligned} \tag{24}$$

This last result proves that the variance of the field with a prescribed spherical covariance, generated by the TBA, as used in HYDRASTAR, is exactly equal to the prescribed variance at every point in the grid, independent of the choice of parameters R, N, and of the directions $\mathbf{l}_i$ of the Turning Bands lines.

In the case of an exponential covariance, from (16), equation (17) becomes

$$C_S(\mathbf{x},\mathbf{x}') = \frac{1}{N}\frac{V}{\sigma_t^2\Sigma}\sum_{i=1}^{N}\sum_{i'=1}^{N}\sum_{k=0}^{8R}\sum_{k'=0}^{8R}E\left[(1-\lambda(k+\frac{1}{2})b)e^{-\lambda kb}(1-\lambda(k'+\frac{1}{2})b)e^{-\lambda k'b}t_{k-j}t_{k-j}\right]. \tag{25}$$

Now, if $i \neq i'$, then t_{k-j} and $t_{k'-j'}$ are independent, and hence

$$E[(1-\lambda(k+\frac{1}{2})b)e^{-\lambda kb}(1-\lambda(k'+\frac{1}{2})b)e^{-\lambda k'b}t_{k-j}t_{k'-j'}] = 0.$$

Therefore

$$C_S(\mathbf{x},\mathbf{x}') = \frac{1}{N}\frac{V}{\sigma_t^2\Sigma}\sum_{i=1}^{N}\sum_{k=0}^{8R}\sum_{k'=0}^{8R}E[(1-\lambda(k+\frac{1}{2})b)e^{-\lambda kb}(1-\lambda(k'+\frac{1}{2})b)e^{-\lambda k'b}t_{k-j}t_{k'-j'}]. \tag{26}$$

Consider

$$\omega = \sum_{k=0}^{8R}\sum_{k'=0}^{8R}E[(1-\lambda(k+\frac{1}{2})b)e^{-\lambda kb}(1-\lambda(k'+\frac{1}{2})b)e^{-\lambda k'b}t_{k-j}t_{k'-j'}].$$

Let $m = k - j$ and let $m' = k' - j'$. Then

$$\omega = \sum_{m=-j}^{8R-j}\sum_{m'=-j'}^{8R-j'}E[(1-\lambda((m+j)+\frac{1}{2})b)e^{-\lambda(m+j)b}(1-\lambda((m'+j')+\frac{1}{2})b)e^{-\lambda(m'+j')b}t_m t_{m'}],$$

$$E[t_m t'_m] = \begin{cases} \sigma_t^2 & \text{if } m = m', \\ 0 & \text{if } m \neq m'. \end{cases}$$

Hence

$$\omega = \sum_{m=MAX(0,j-j')}^{MIN(8R,8R+j-j')}\sigma_t^2(1-\lambda((m+j)+\frac{1}{2})b)e^{-\lambda(m+j)b}(1-\lambda((m+j')+\frac{1}{2})b)e^{-\lambda(m+j')b},$$

$$= \sum_{k=MAX(0,j-j')}^{MIN(8R,8R+j-j')} \sigma_t^2(1-\lambda((k)+\frac{1}{2})b)e^{-\lambda(k)b}(1-\lambda((k-j+j')+\frac{1}{2})b)e^{-\lambda(k-j+j')b}.$$

Therefore

$$C_S(\mathbf{x},\mathbf{x}') = \frac{1}{N}\frac{V}{\sigma_t^2\Sigma}\sum_{i=1}^{N}\sum_{k=MAX(0,j-j')}^{MIN(8R,8R+j-j')} \sigma_t^2(1-\lambda((k)+\frac{1}{2})b)e^{-\lambda(k)b}(1-\lambda((k-j+j')+\frac{1}{2})b)e^{-\lambda(k-j+j')b}. \tag{27}$$

Equation (27) gives the covariance of the ensemble of realizations of a field with a prescribed exponential covariance, generated by the TBA as implemented in HYDRASTAR. The equation is valid for any values of the parameters R, N, and of the directions $\mathbf{l}_i$ of the Turning Bands lines.

A special case arises when $\mathbf{x} = \mathbf{x}'$. In this case, $j = j'$, and

$$\begin{aligned} Var(\mathbf{x}) &= \frac{1}{N}\frac{V}{\sigma_t^2\Sigma}\sum_{i=1}^{N}\sum_{k=0}^{8R}\sigma_t^2(1-\lambda((k)+\frac{1}{2})b)^2e^{-2\lambda(k)b}, \\ &= \frac{V}{\sigma_t^2\Sigma}\sum_{k=0}^{8R}\sigma_t^2(1-\lambda((k)+\frac{1}{2})b)^2e^{-2\lambda(k)b}, \\ &= V. \end{aligned} \tag{28}$$

This last result proves that the variance of the field with a prescribed exponential covariance, generated by the TBA, as used in HYDRASTAR, is exactly equal to the prescribed variance at every point in the grid, independent of the choice of parameters R, N, and of the directions $\mathbf{l}_i$ of the Turning Bands lines.

As part of this study, the expressions derived for the covariance, equations (23) and (27), were evaluated numerically for different values of the parameters R and N. The covariance is dependent on the directions of the Turning Bands lines. In HYDRASTAR, these lines are generated as sets of 15 lines joining the mid-points of the opposite edges of a regular icosahedron. The sets are randomly orientated in three-dimensional space. The resulting covariance is therefore not isotropic, because of the finite number of lines. For a representative randomly-generated set of line orientations, the ensemble covariance averaged over all directions as a function of separation, and also the magnitude of the largest error in the covariance were calculated.

Figures 2.2 and 2.3 show how the direction-averaged covariance varies with separation, as a function of the parameters R and N. These plots demonstrate that the error in the direction-averaged covariance is relatively small, particularly for the exponential covariance model. The size of the error depends mainly on the value of the parameter R, rather than on the number of icosahedron sets of lines. In fact,

the error is not greatly reduced by increasing the number of lines beyond 15. The error is significantly smaller for the exponential covariance model, compared with the spherical model, presumably because more points are used to evaluate the moving average in the exponential model, for a given value of R.

Finally, the maximum error (that is, the magnitude of the difference between the prescribed value and the calculated value) in the ensemble-averaged covariance was calculated for a representative randomly-generated orientation of the Turning Bands lines. This was done for various values of the parameters R and N. These errors are a pessimistic measure of the quality of the generated fields, since they occur at particular directions only, and are much greater than the errors averaged over all directions. Nevertheless, they do measure the distortion effect due to a finite number of lines, and may be an important consideration when modelling certain types of physical phenomena [5]. These maximum errors are shown in the Table 2.1 below.

Covariance model	R=20 1 set	R=20 4 sets	R=100 1 set	R=100 4 sets
Spherical	0.33	0.13	0.33	0.13
Exponential	0.33	0.10	0.33	0.09

Table 2.1: Table showing the maximum errors in the covariance for particular randomly-generated orientations of the Turning Bands lines. In each case the grid consisted of 30x30x30 points, with a range parameter of $a = 10$ grid spacings in the spherical case, or $\lambda = 3.3$ grid spacings in the exponential case.

Figures 2.5, 2.6, 2.8 and 2.9 show the ensemble-averaged covariance of the fields generated by the TBA, plotted on a slice through the origin of the three-dimensional grid. These should be compared with Figures 2.4 and 2.7 which show the equivalent exact spherical and exponential covariance functions. The plots show how the covariance changes for different numbers of icosahedron sets, for the spherical and exponential covariance models. The linelike distortions are clearly evidenced, particularly when only a single icosahedron set is used. With 4 sets of lines, the distortion effect is much less visible.

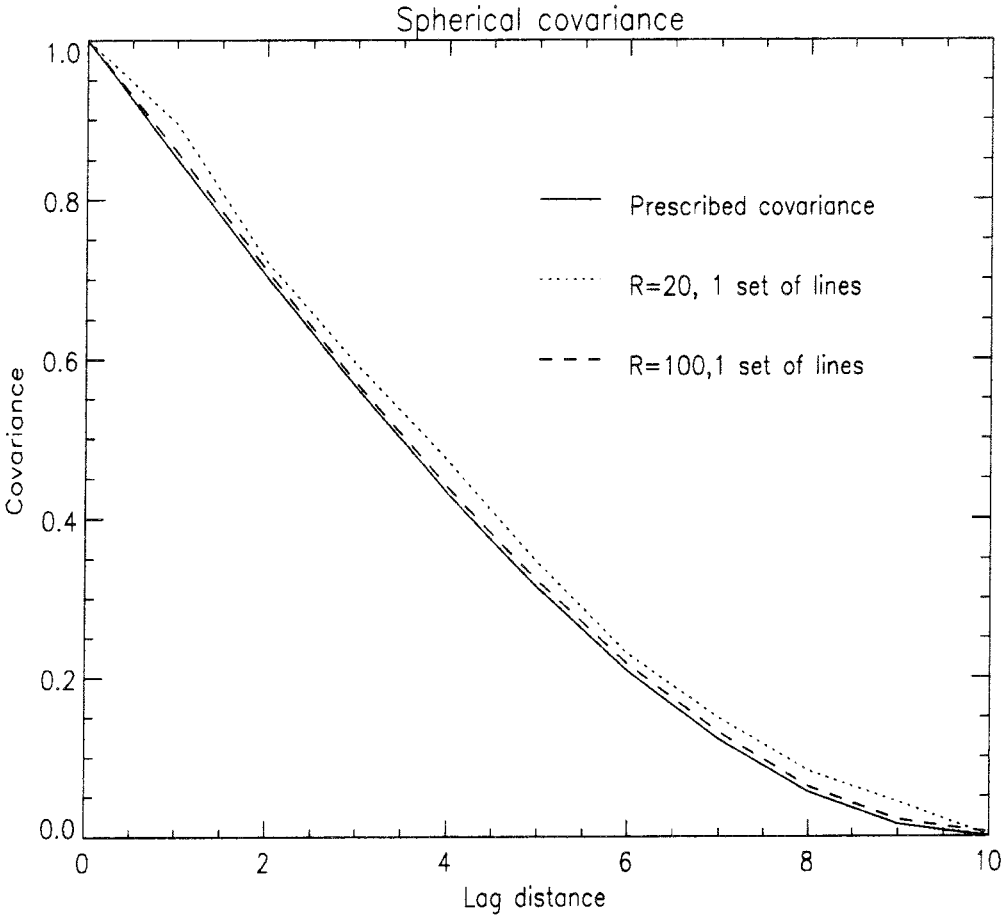

Figure 2.2: Plot of the direction-averaged ensemble covariance generated by the Turning Bands method as implemented in HYDRASTAR. The prescribed covariance is spherical with a range of $a = 10$.

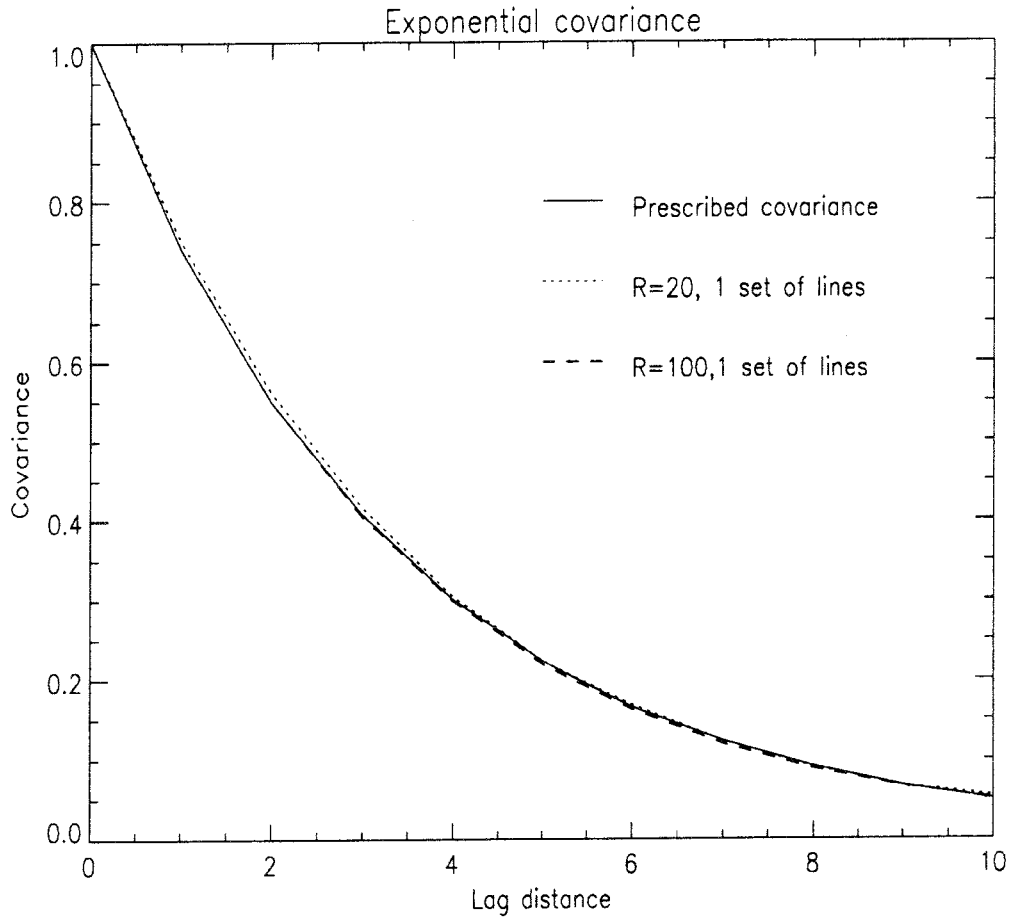

Figure 2.3: Plot of the direction-averaged ensemble covariance generated by the Turning Bands method as implemented in HYDRASTAR. The prescribed covariance is exponential with a range of $\lambda = 3.3$.

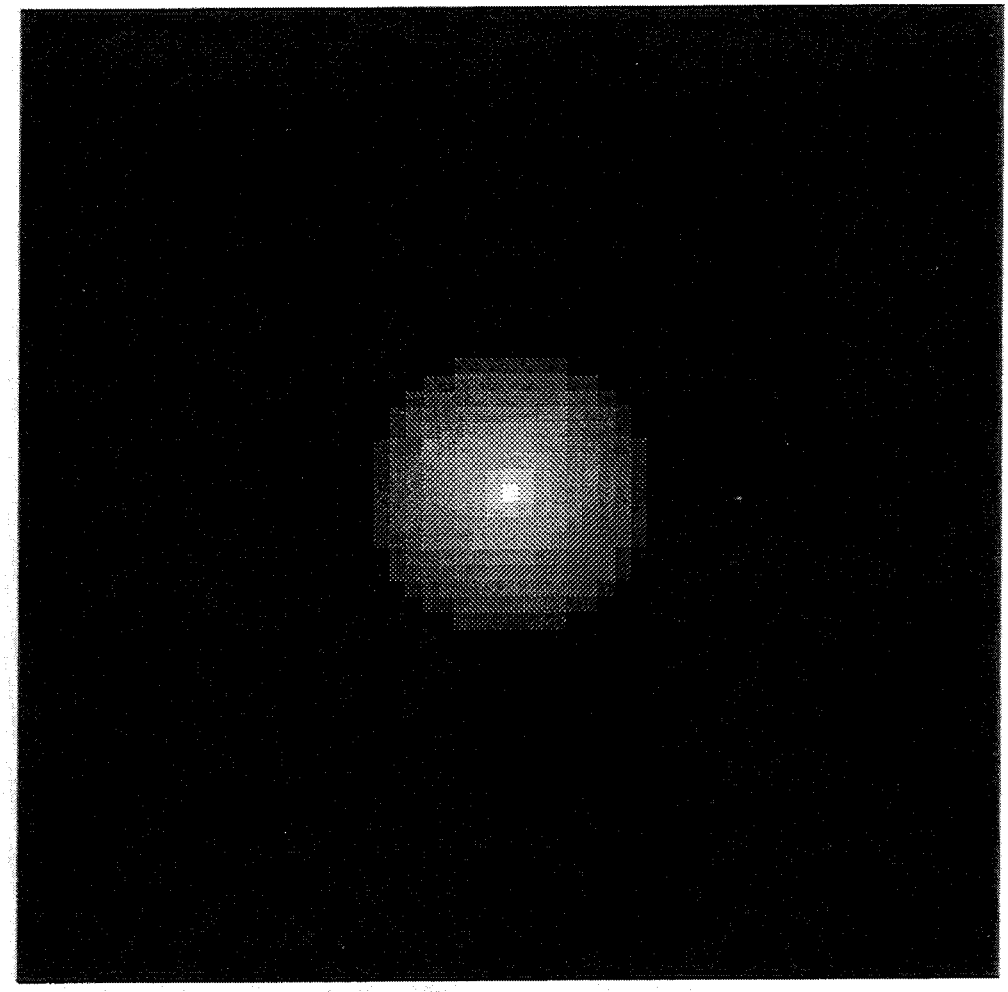

Figure 2.4: Plot of the exact spherical covariance function with a range of $a = 10$ grid spacings, plotted on a slice through the origin of a three-dimensional grid; black represents a covariance of zero, white represents a covariance of one. The grid consisted of $30 \times 30 \times 30$ points.

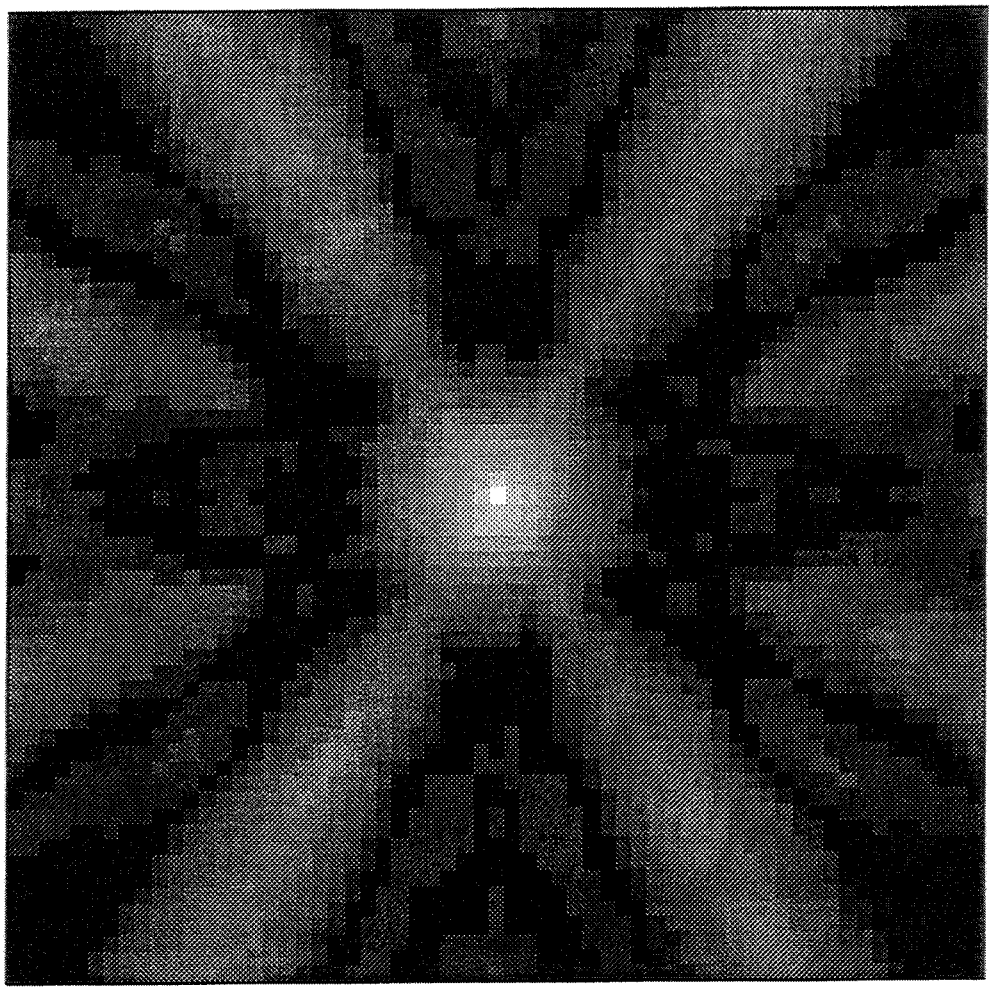

Figure 2.5: Plot of the ensemble-averaged covariance generated by the Turning Bands method as implemented in HYDRASTAR. The covariance is plotted on a slice through the origin of the three-dimensional grid; black represents a covariance of zero, white represents a covariance of one. The grid consisted of $30 \times 30 \times 30$ points with a spherical covariance of range $a = 10$ grid spacings. One set of lines was used and the value of R was 20.

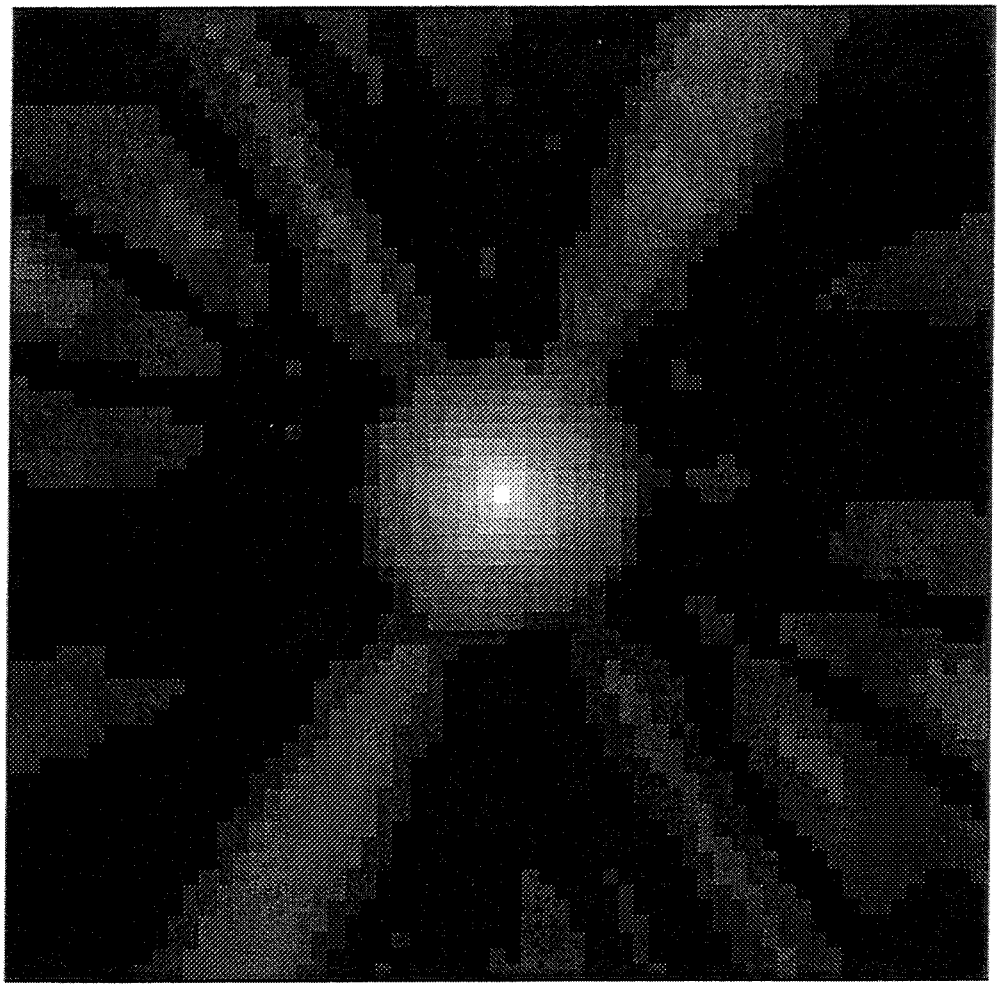

Figure 2.6: Plot of the ensemble-averaged covariance generated by the Turning Bands method as implemented in HYDRASTAR. The covariance is plotted on a slice through the origin of the three-dimensional grid; black represents a covariance of zero, white represents a covariance of one. The grid consisted of $30 \times 30 \times 30$ points with a spherical covariance of range $a = 10$ grid spacings. Four sets of lines were used and the value of R was 20.

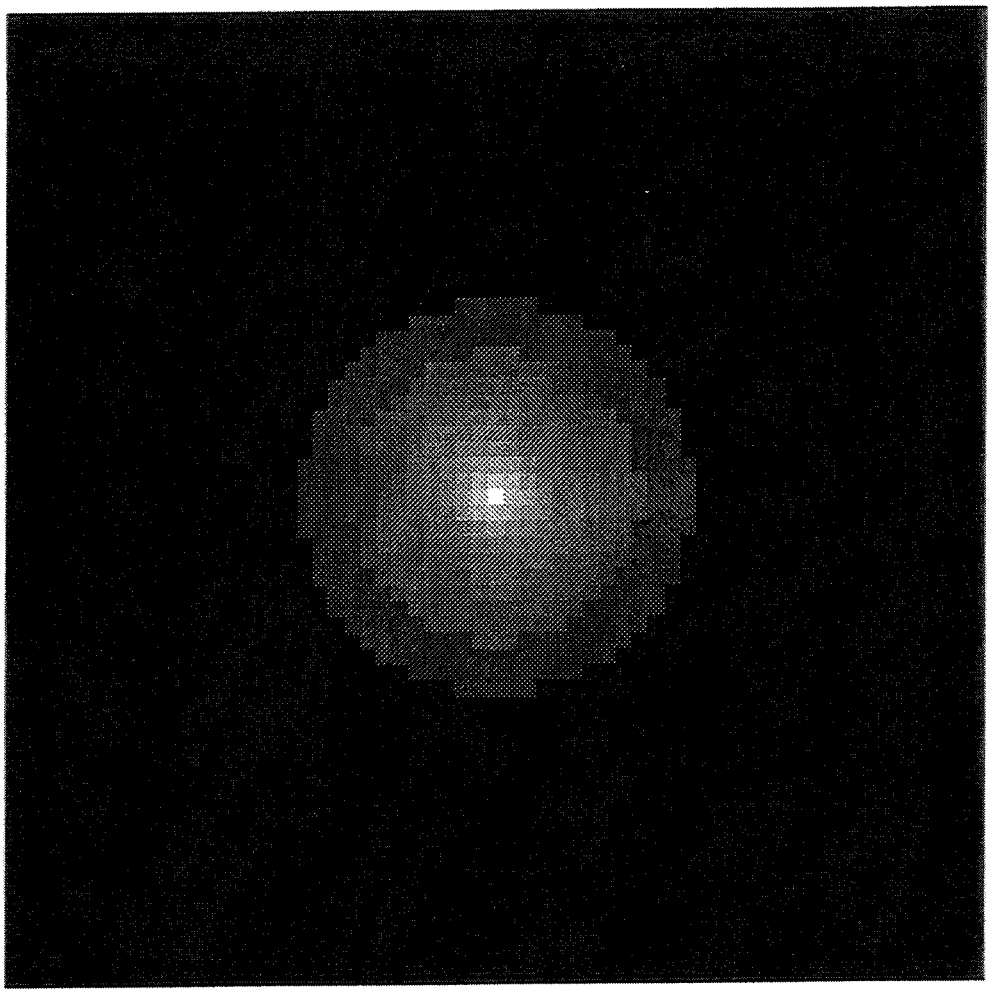

Figure 2.7: Plot of the exact exponential covariance function with a range of $\lambda = 3.3$ grid spacings, plotted on a slice through the origin of a three-dimensional grid; black represents a covariance of zero, white represents a covariance of one. The grid consisted of $30 \times 30 \times 30$ points.

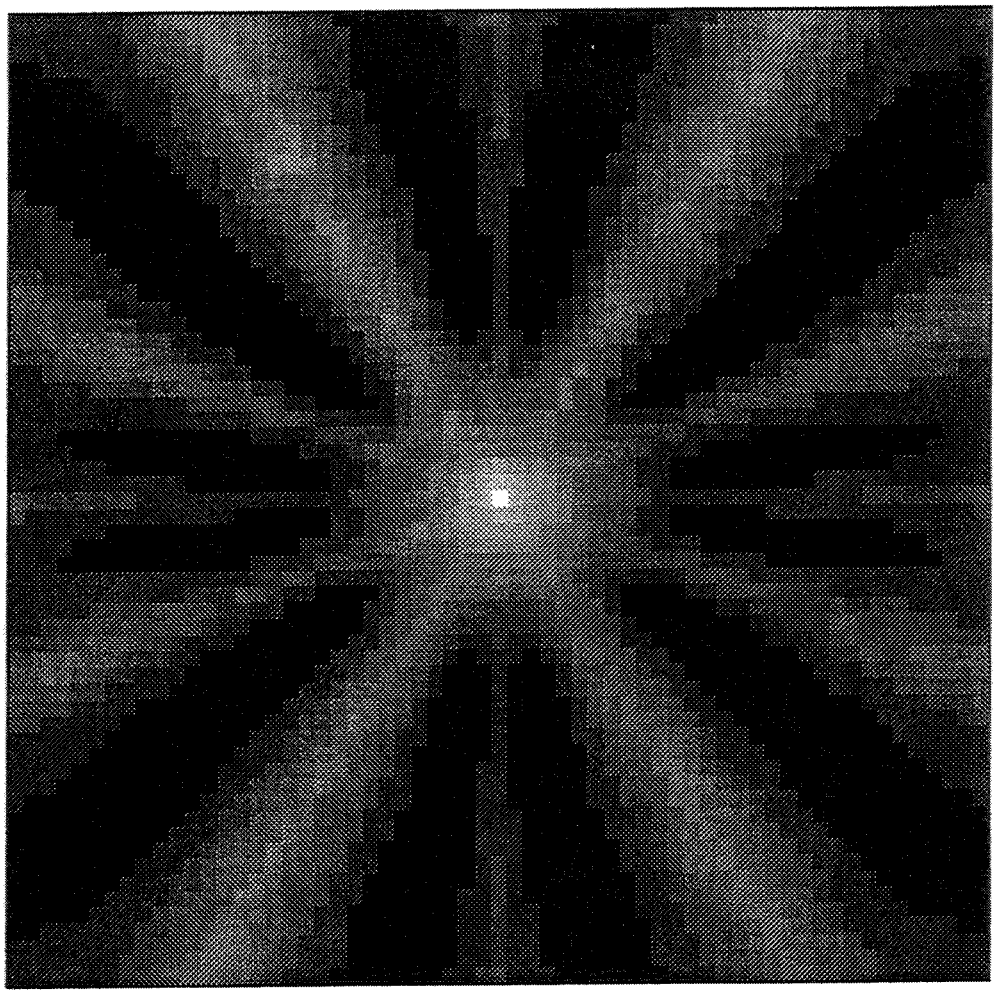

Figure 2.8: Plot of the ensemble-averaged covariance generated by the Turning Bands method as implemented in HYDRASTAR. The covariance is plotted on a slice through the origin of the three-dimensional grid; black represents a covariance of zero, white represents a covariance of one. The grid consisted of $30 \times 30 \times 30$ points with an exponential covariance of range $\lambda = 3.3$ grid spacings. One set of lines was used and the value of R was 20.

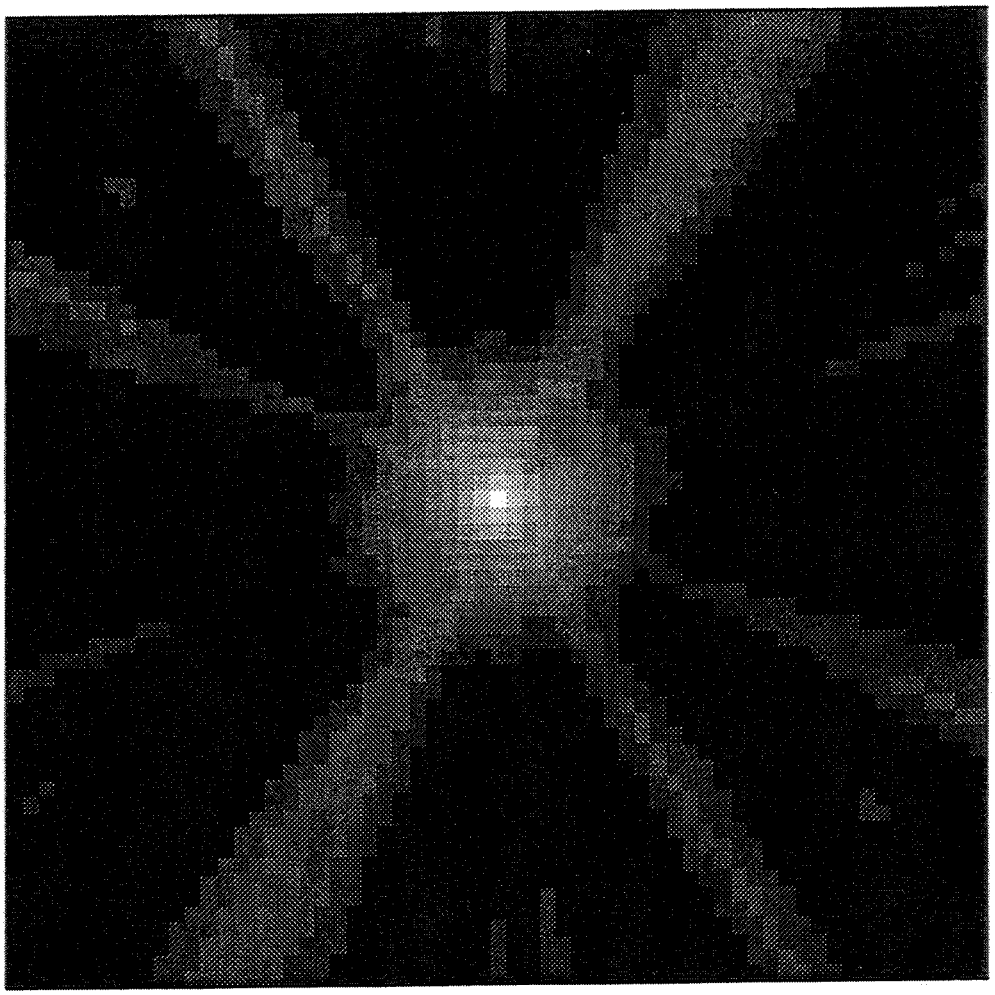

Figure 2.9: Plot of the ensemble-averaged covariance generated by the Turning Bands method as implemented in HYDRASTAR. The covariance is plotted on a slice through the origin of the three-dimensional grid; black represents a covariance of zero, white represents a covariance of one. The grid consisted of $30 \times 30 \times 30$ points with an exponential covariance of range $\lambda = 3.3$ grid spacings. Four sets of lines were used and the value of R was 20.

2.4 Summary and Conclusions

This study has investigated in detail the Turning Bands algorithm as implemented in HYDRASTAR. Analytic expressions have been derived for the ensemble mean, variance and covariance of the generated fields for both the spherical and exponential covariance models. The results indicate that with the values of the parameters recommended by Norman [3] the mean, variance and covariance of the generated fields, with either exponential or spherical covariance, are sufficiently accurate for most practical purposes.

For both models, the ensemble mean and variance of the generated fields were found to be exactly as prescribed, for any point in the grid, for any discretization, and for any number and orientation of lines. There is some evidence of striping, or direction-dependent effects in the covariance due to the finite number of lines, but the effect is small and the maximum error in the covariance is approximately 13% of the variance for the spherical case, and 10% for the exponential case. These errors are probably acceptably small, but could be reduced if necessary by increasing the number of lines. The error in the direction-averaged covariance was found to be very small, approximately 3% of the variance in the spherical case, and 1% in the exponential case.

It is concluded that the Turning Bands algorithm, as implemented in HYDRASTAR accurately generates fields with the prescribed mean, variance and covariance, for both spherical and exponential covariance models, provided that 4 sets of icosahedron lines with the parameter values recommended by Norman [3] are used.

3. DISPERSION IN TWO DIMENSIONS: SMALL VARIANCE

3.1 Description of the Test Case

In the second part of this verification study, the case of uniform mean flow in two dimensions with small variance of the hydraulic conductivity field was investigated. This is a useful case from the point of view of verification, since an analytic solution exists for the first and second order moments of velocity and of particle displacement in this case [10], [7]. The analytic solutions are valid for small variance. In this section, the calculations made using HYDRASTAR are described, and the results obtained are compared with the analytic results.

The methodology for making this type of calculation is as follows. Firstly, a random realization of the hydraulic conductivity field with a constant mean and a specified covariance is generated. Next the flow field is calculated for this realization, with hydraulic head boundary conditions which would support a uniform flow solution in the case of a constant hydraulic conductivity. A particle tracking algorithm is used to calculate the advective transport. These calculations are repeated for a large number of independent realizations, in order to estimate the statistics for the ensemble of possible realizations. The uncertainty due to the finite number of realizations can also be estimated from the results.

HYDRASTAR calculates flow and transport in a three-dimensional medium. The approach adopted in this study to modelling two-dimensional flow and transport was to specify the grid length in the third direction to be much smaller than in the other two directions, and also much smaller than the correlation length of the hydraulic conductivity field. Using a uniform head gradient in the first direction, and no-flow boundaries in the other two directions, this approach ensured that there was effectively no flow in the third direction. Figure 3.1 shows the domain and boundary conditions used in the test case.

The physical parameters used in the study are as shown in Table 3.1. The large bandwidth factor was chosen because of the different grid scales used in each direction. The bandwidth, that is the width of the Turning Bands, is equal to the product of the bandwidth factor and the minimum grid spacing. The grid spacing in the third direction in this case was 500 times smaller than the grid spacing in the other two directions. Hence, a bandwidth factor of 100 corresponds to choosing a bandwidth of 0.2 times the grid spacing in the first and second directions. The variance of the logarithm (to base 10) of the hydraulic conductivity was chosen to be 0.1886. This

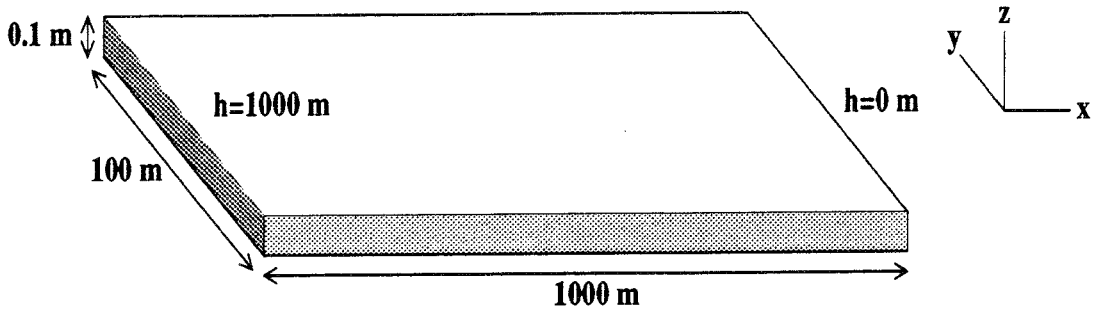

Figure 3.1: Domain and boundary conditions used for the two-dimensional calculation. h is the hydraulic head.

Grid dimensions	1000m x 1000m x 0.1m
Covariance model	exponential
Range parameter, λ	33.3m
Number of head nodes	121x121x4
Bandwidth factor	100.0
Number of sets of lines	4
Mean head gradient	1.0
Principal components of hydraulic conductivity	1.0, 1.0, 1.0
Porosity	0.1
Residual tolerance (used in HYDROGEOLOGY_EQ block)	1.0E-6
Tolerance (used in TRANSPORT block)	0.2

Table 3.1: Physical parameters used for the two-dimensional study at small variance. The residual tolerance is used as a criterion for terminating the conjugate gradient iterations when solving the groundwater equation. The tolerance used in the TRANSPORT block defines the maximum step length.

corresponds to a variance of 1.0 in natural logarithms. The analytical results are expected to remain valid up to a variance of around 1.0, in natural logarithms. No conditioning data were used since the study was intended to address the case of flow in a generic rock formation. The analytical results are applicable only for cases without conditioning. The flow and transport were calculated for a total of 100 realizations of the hydraulic conductivity field. The HYDRASTAR input file used in this case is shown in Appendix A.

3.2 Flow Calculations

The statistics of the velocity field were calculated using the RESULT_ESTIMATION block of HYDRASTAR. Table 3.2 shows the mean Darcy velocity in the longitudinal and transverse directions. These results are in reasonable agreement with the velocity calculated using the assumption that the effective hydraulic conductivity is equal to the prescribed mean hydraulic conductivity.

Direction	Theoretical	Calculated
x	1.0 ms^{-1}	1.23 ms^{-1}
y	0.0 ms^{-1}	-0.0003 ms^{-1}

Table 3.2: Mean Darcy velocity in the longitudinal and transverse directions for the two-dimensional simulations at small variance.

For the case of small variance, Rubin [10] has calculated analytically the variogram of the fluctuation of the Darcy velocity about the mean. This analytic calculation is based on the earlier work of Dagan [7], and uses the same assumptions. It is therefore a useful additional quantity to examine in order to test that HYDRASTAR calculates the groundwater flow correctly.

The current output options of HYDRASTAR only allow the variogram of the velocity components themselves to be calculated; not the difference between the velocity and the mean. However, since the mean transverse velocity is zero, the variogram of the transverse velocity calculated by HYDRASTAR can be compared with the analytical expression for the variogram of transverse velocity fluctuation. Being a second-order transverse quantity, it is expected to depend sensitively on the details of the flow calculation, and is therefore very valuable from the point of view of verification.

Rubin's paper contains a number of errors which were corrected as part of the

present study. Table 3.2 shows how the calculated normalized variogram of transverse velocity varies as a function of separation, compared with the corrected version of the analytic results derived by Rubin. The calculated results can be seen to be in good agreement with the analytic results.

Separation	Rubin	HYDRASTAR
0λ	0.0	0.0
0.5λ	0.18	0.18
1.5λ	0.23	0.21
2.5λ	0.25	0.21
3.5λ	0.26	0.21
4.5λ	0.26	0.21

Table 3.3: Normalized variogram of the transverse velocity calculated by HYDRASTAR as a function of separation compared with the corrected version of the analytical results derived by Rubin.

3.3 Transport Calculations

HYDRASTAR calculates the transport of solutes using a particle-tracking approach. Particles move due to advection alone, and all dispersion is due to the spatial variations in the flow field. Molecular diffusion, and dispersion at a scale smaller than the grid spacing is neglected. In the calculations reported here, a starting position for the particle-tracking of 3λ from the leftmost boundary was used. This was assumed to be sufficient to avoid any significant boundary effects.

The results from such particle-tracking calculations can be compared directly with the analytic results of Dagan [7], which are valid for small variance. Dagan calculated expressions for the second-order longitudinal and transverse moments of particle displacement as a function of time. Dagan's expressions for the variances of longitudinal and transverse displacement, X_{11} and X_{22} are

$$\frac{X_{11}}{\sigma^2\lambda^2} = 2t' - 3\ln t' + \frac{3}{2} - 3E + 3\left[Ei(-t') + \frac{e^{-t'}(1+t') - 1}{t'^2}\right], \tag{29}$$

$$\frac{X_{22}}{\sigma^2\lambda^2} = \ln t' - \frac{3}{2} + E - Ei(-t') + 3\left[\frac{1-(1+t')e^{-t'}}{t'^2}\right], \tag{30}$$

where E is the Euler number, $E = 0.577...$, Ei is the exponential integral, and t' is the normalized time, $t' = t\bar{v}/\lambda$, where $\bar{v}$ is the mean groundwater speed, and λ is the range parameter of the logarithm of the hydraulic conductivity field.

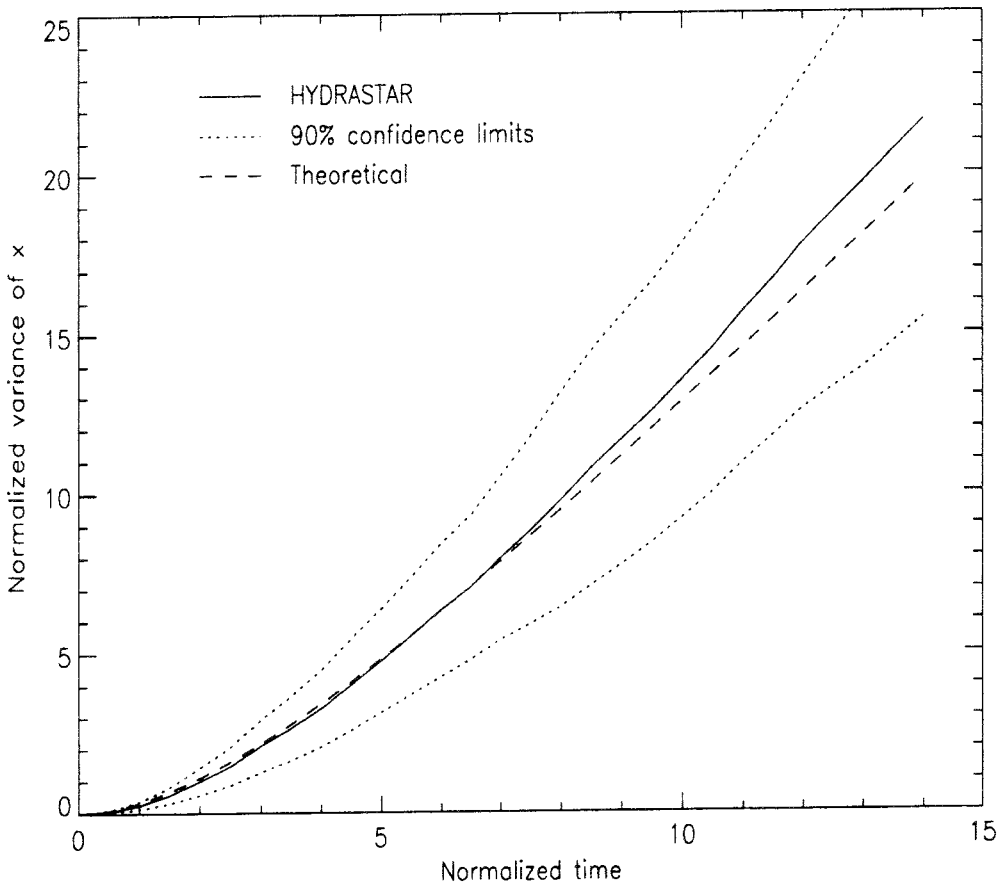

Figure 3.2: Plot of the normalized variance of the longitudinal displacement as a function of normalized time, for the case of two-dimensional flow and small variance of the logarithm of hydraulic conductivity. The 90% Guttman bounds and Dagan's analytical result are also plotted.

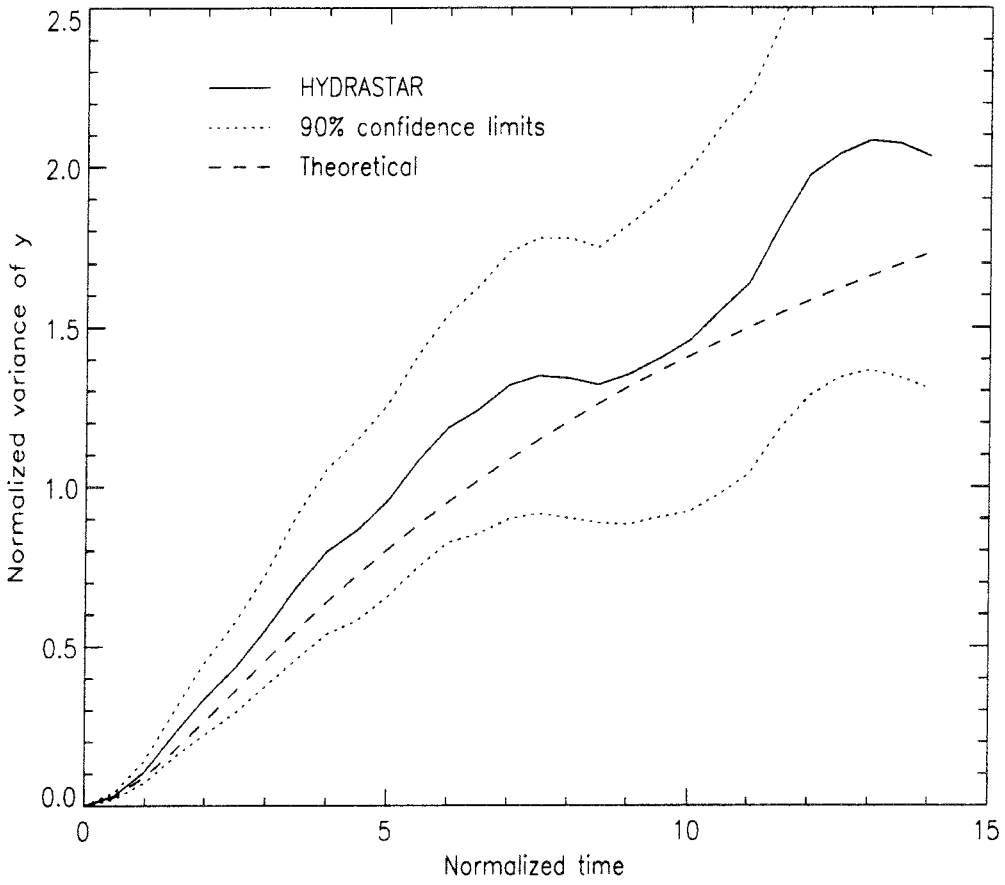

Figure 3.3: Plot of the normalized variance of the transverse displacement as a function of normalized time, for the case of two-dimensional flow and small variance of the logarithm of hydraulic conductivity. The 90% Guttman bounds and Dagan's analytical result are also plotted.

Figures 3.2 and 3.3 show how the results calculated using HYDRASTAR compare with Dagan's analytic results, for both the longitudinal and transverse cases. In these figures the variances of displacement are normalized by dividing by $\sigma^2\lambda^2$, as in (29) and (30). The confidence limits include only the uncertainty due to the finite number of realizations, and ignore errors due to the finite grid size, finite time step, boundary effects and the finite number of particles. Nevertheless, for this small value of the variance, the statistical errors are believed to be the dominant source of uncertainty [11]. The confidence limits are calculated using Guttmann's inequality [12], which makes no assumption about whether the particle displacement moments follow a normal distribution, or indeed any other type of distribution. It is clear from the figures that the calculated results are in very good agreement with the analytic results, the analytic results being well within the 90% confidence bounds.

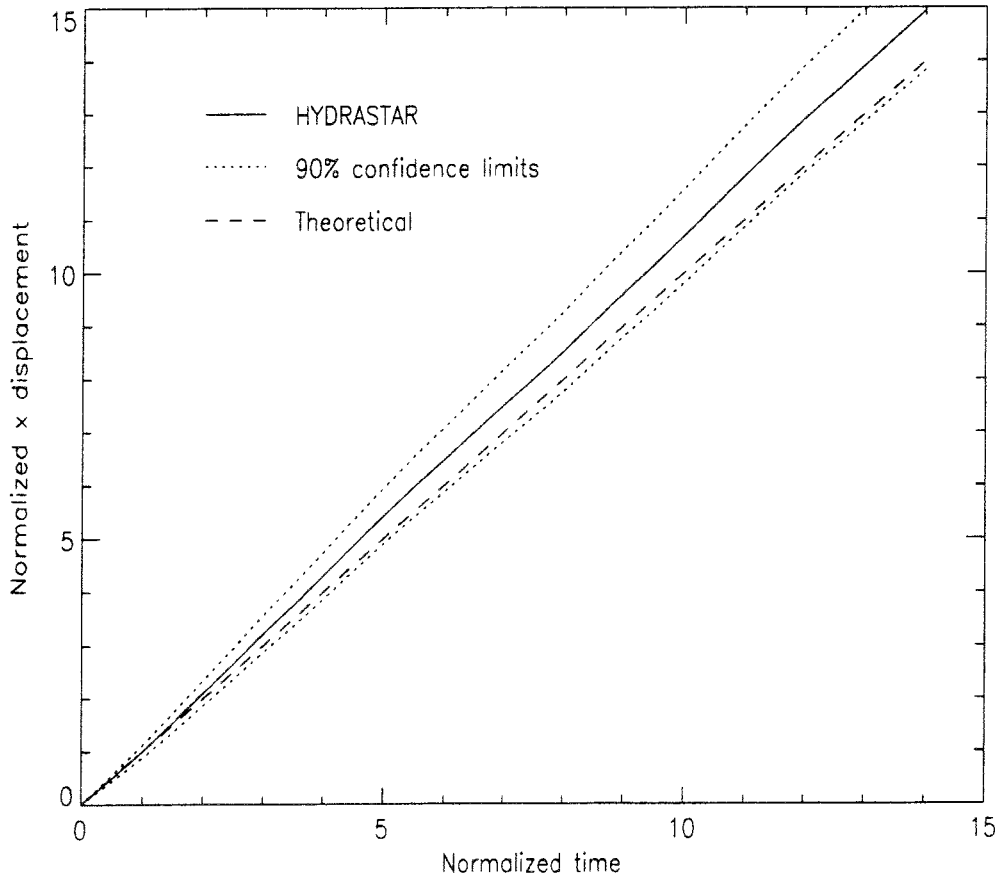

Figure 3.4: Plot of the normalized longitudinal displacement as a function of normalized time, for the case of two-dimensional flow and small variance of the logarithm of hydraulic conductivity. The 90% Guttman bounds are plotted and the theoretical result is also plotted for reference.

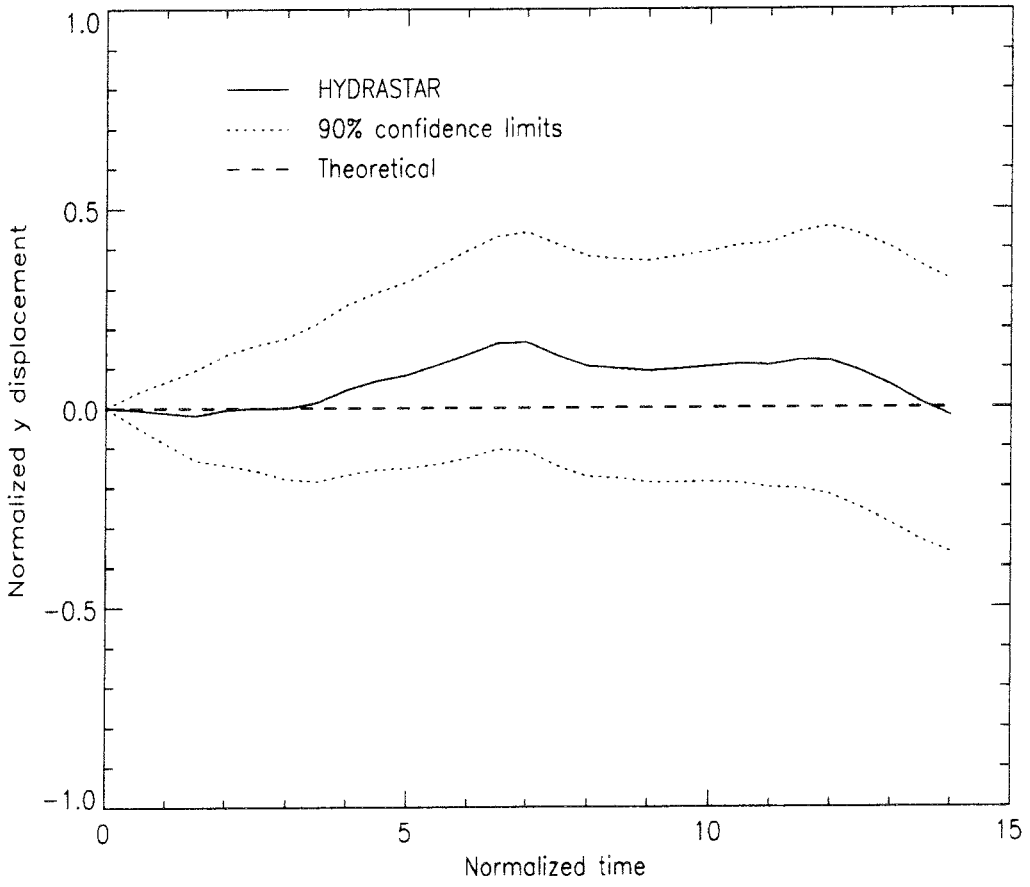

Figure 3.5: Plot of the normalized transverse displacement as a function of normalized time, for the case of two-dimensional flow and small variance of the logarithm of hydraulic conductivity. The 90% Guttman bounds are plotted and the theoretical result is also plotted for reference.

Figures 3.4 and 3.5 show how the mean longitudinal and transverse displacements vary as a function of time. In these plots, both the time and the displacement are normalized with respect to the correlation length. As expected, the mean longitudinal displacement is proportional to time, with a mean speed approximately equal to the mean speed calculated by assuming that the effective hydraulic conductivity is equal to the prescribed mean hydraulic conductivity. The mean transverse displacement is found to be approximately zero at all times, as expected.

3.4 Conclusions

The results calculated using HYDRASTAR are generally in good agreement with the results expected from theoretical considerations. In particular, the moments of particle displacement are seen to be in very good agreement with the analytic results of Dagan, which are valid for small variance. These moments are a very sensitive measure, and so this indicates strongly that HYDRASTAR is capable of calculating accurately both the flow and transport in this two-dimensional case with small variance of the logarithm of hydraulic conductivity.

4. DISPERSION IN TWO DIMENSIONS: MODERATE VARIANCE

4.1 Description of Test Case

Next, the case of uniform mean flow in two dimensions with a moderate variance of the hydraulic conductivity field was investigated. In this case the analytic solution for the first and second order moments of the particle displacement may not be valid. In order to verify the results obtained by HYDRASTAR for this case, a similar calculation was made using the SPV2D program developed by AEA Technology [13]. This is a two-dimensional finite volume program which solves the groundwater flow equations in a rectangular domain, and which calculates transport using a particle tracking method. A linear interpolation scheme is used to obtain the velocities used by the particle tracking method. In this section, the calculations made using HYDRASTAR are described, and the results obtained are compared with the numerical results obtained using SPV2D.

The geometry and boundary conditions used in this case were essentially the same as for the case of small variance of the hydraulic conductivity field, except that a larger domain and smaller mesh size were used. In the case of moderate variance the numerical errors in the solution of the groundwater flow equation are larger on a given mesh, and so a finer discretization of the computational mesh is required to give the same size of discretization error. In this study, a grid refinement of 8 nodes per correlation scale, λ, was used, compared with a refinement of 4 nodes per correlation scale for the small variance case. The parameters used in this case are as shown in Table 4.1. A larger domain size was required because of the increased dispersion at this larger variance.

The variance of the logarithm (to base 10) of the hydraulic conductivity was chosen to be 0.943. This corresponds to a variance of 5.0 in natural logarithms. As before, no conditioning data was used. The flow and transport were calculated for a total of 241 realizations. More realizations are needed in this case of moderate variance, because the statistical variation in the results is greater than in the case of small variance. Therefore more realizations are needed in order to obtain equally reliable statistics. Also many more conjugate gradient iterations were needed to solve the flow equation. The HYDRASTAR input file used in this case is shown in Appendix B.

The calculations using SPV2D were carried out using the same domain size and grid refinement as the HYDRASTAR calculations, except that SPV2D uses a

Grid dimensions	1332m x 832.5 x 0.1m
Covariance model	exponential
Range parameter, λ	33.3m
Number of head nodes	301x201x4
Bandwidth factor	25.0
Number of sets of lines	4
Mean head gradient	1.0
Principal components of hydraulic conductivity	1.0, 1.0, 1.0
Porosity	0.1
Residual tolerance (used in HYDROGEOLOGY_EQ block)	1.0E-6
Tolerance (used in TRANSPORT block)	0.2

Table 4.1: Physical parameters used for the two-dimensional study at moderate variance.

strictly two-dimensional grid. In this case, 50 lines with orientations drawn at random from a uniform distribution were used instead of the 4 icosahedron sets of lines used by HYDRASTAR. The realizations of the hydraulic conductivity field should be satisfactory in either case. The mean head gradient, mean hydraulic conductivity, and porosity were as in the HYDRASTAR calculation. The number of realizations was 250 in this case.

4.2 Transport Calculations

The analytical results of Dagan are expected to remain valid up to a variance of around 1.0, in natural logarithms. For a variance of 5.0, some deviation from Dagan's results may be expected. Hartley and Morris [11] showed that for variances larger than 1, Dagan's result tends to over-predict the second-order moments of particle displacement in both the longitudinal and transverse directions. The amount of deviation is expected to be significant for a variance of 5.0.

Figures 4.1 and 4.2 show how the longitudinal and transverse moments calculated using HYDRASTAR compare with the results from SPV2D, using the same mesh. Dagan's analytic results are also plotted for comparison. The confidence limits include only the statistical uncertainty due to the finite number of realizations. Hartley and Morris showed that for this moderate value of the variance, other errors due to the finite grid size, finite time step, and boundary effects are likely to be of a similar size to the statistical errors. The confidence limits plotted in these figures

should therefore be regarded as optimistic. It can be seen that the results calculated using HYDRASTAR are reasonably consistent with those calculated using SPV2D.

Figure 4.3 also shows how the mean normalized longitudinal displacement varies as a function of normalized time for the two calculations. In both cases the mean longitudinal displacement is proportional to time, with a mean speed approximately equal to the mean speed calculated by assuming that the effective hydraulic conductivity is equal to the prescribed mean hydraulic conductivity. The mean transverse displacements are found to be approximately zero at all times, as expected.

4.3 Conclusions

The calculations at moderate variance are less conclusive than in the case of small variance. This is due to the greatly increased size of the numerical errors, resulting in greater uncertainty. As shown by Hill [14], the error in the calculation of velocity is proportional to the square root of the mesh spacing. This slow rate of convergence means that the error in the velocity and in the particle displacement may be significant even for very refined meshes. This implies that very highly refined meshes would be needed to obtain accurate results for the case of large variances. Results obtained using coarse meshes may bear little resemblance to those obtained using more refined meshes.

Nevertheless, the results calculated using HYDRASTAR using this test case are reasonably consistent with similar results calculated using the program SPV2D. This helps to build confidence in HYDRASTAR, since the two programs have been developed independently, and do not use identical numerical algorithms.

The results of this section indicate the potential difficulties of obtaining accurate results for the case of large variance. Because of the need for more refined meshes, more realizations, and more iterations, the computation time needed is significantly greater than for the small variance case. This may place practical limits on the size of the variance that can be studied.

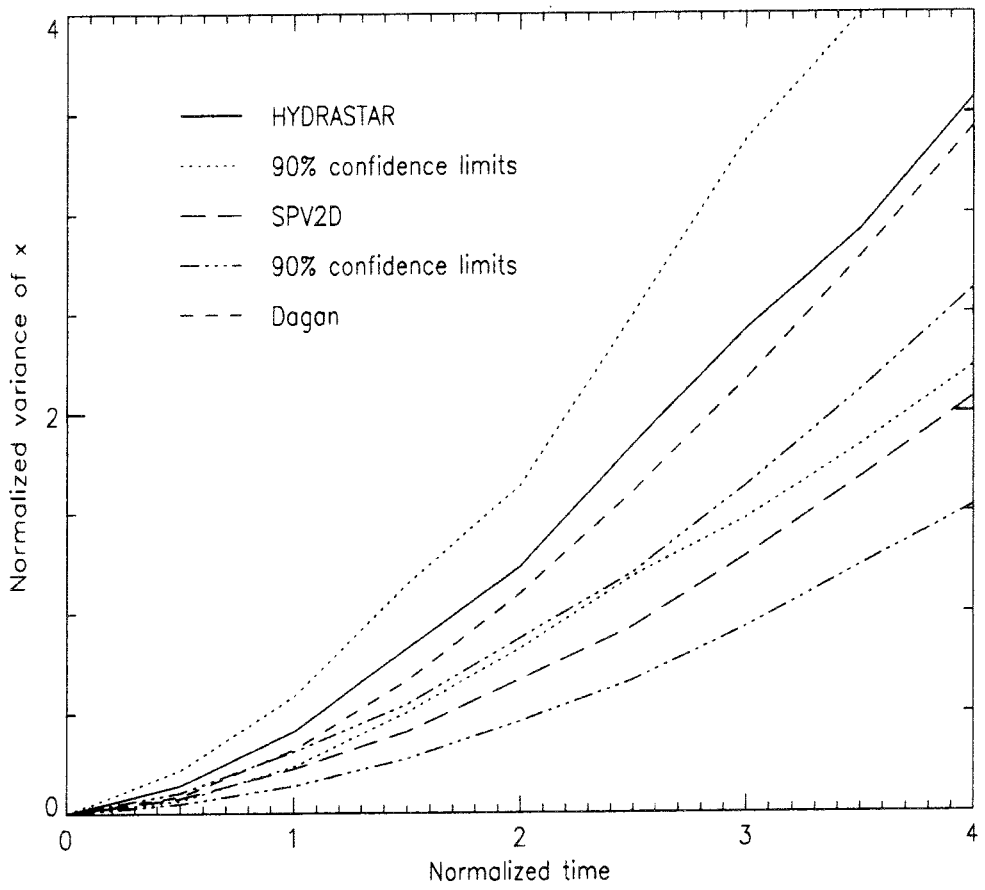

Figure 4.1: Plot of the normalized variance of the longitudinal displacement as a function of normalized time, for the case of two-dimensional flow and moderate variance of the logarithm of hydraulic conductivity. The results obtained using the program SPV2D are also plotted, together with the 90% Guttman bounds and Dagan's analytical result.

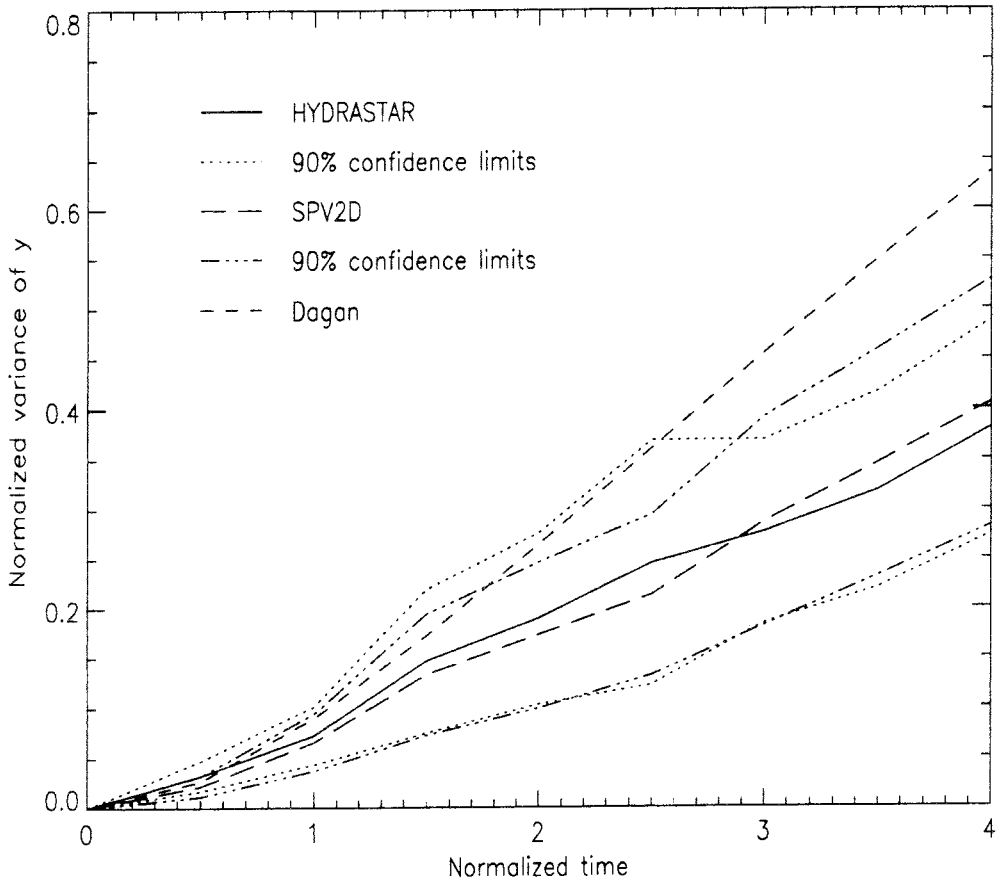

Figure 4.2: Plot of the normalized variance of the transverse displacement as a function of normalized time, for the case of two-dimensional flow and moderate variance of the logarithm of hydraulic conductivity. The results obtained using the program SPV2D are also plotted, together with the 90% Guttman bounds and Dagan's analytical result.

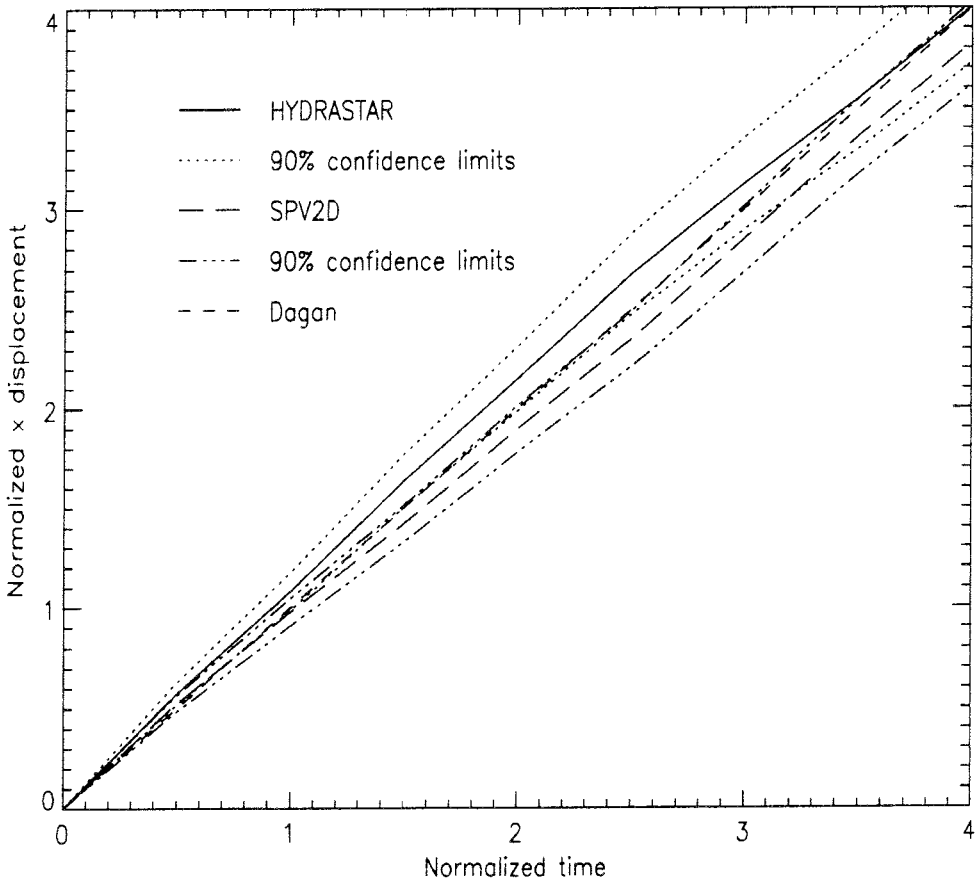

Figure 4.3: Plot of the normalized longitudinal displacement as a function of normalized time, for the case of two-dimensional flow and moderate variance of the logarithm of hydraulic conductivity. The results obtained using the program SPV2D are also plotted, together with the 90% Guttman bounds and the expected result.

5. DISPERSION IN THREE DIMENSIONS: SMALL VARIANCE

5.1 Description of Test Case

In the final part of this verification study, the case of uniform mean flow in three dimensions with small variance of the hydraulic conductivity field was investigated. As in the two-dimensional case, an analytic solution has been derived for the first and second order moments of particle displacement in this three-dimensional case [7]. In this section, the calculations made using HYDRASTAR are described, and the results obtained are compared with the analytic results obtained by Dagan.

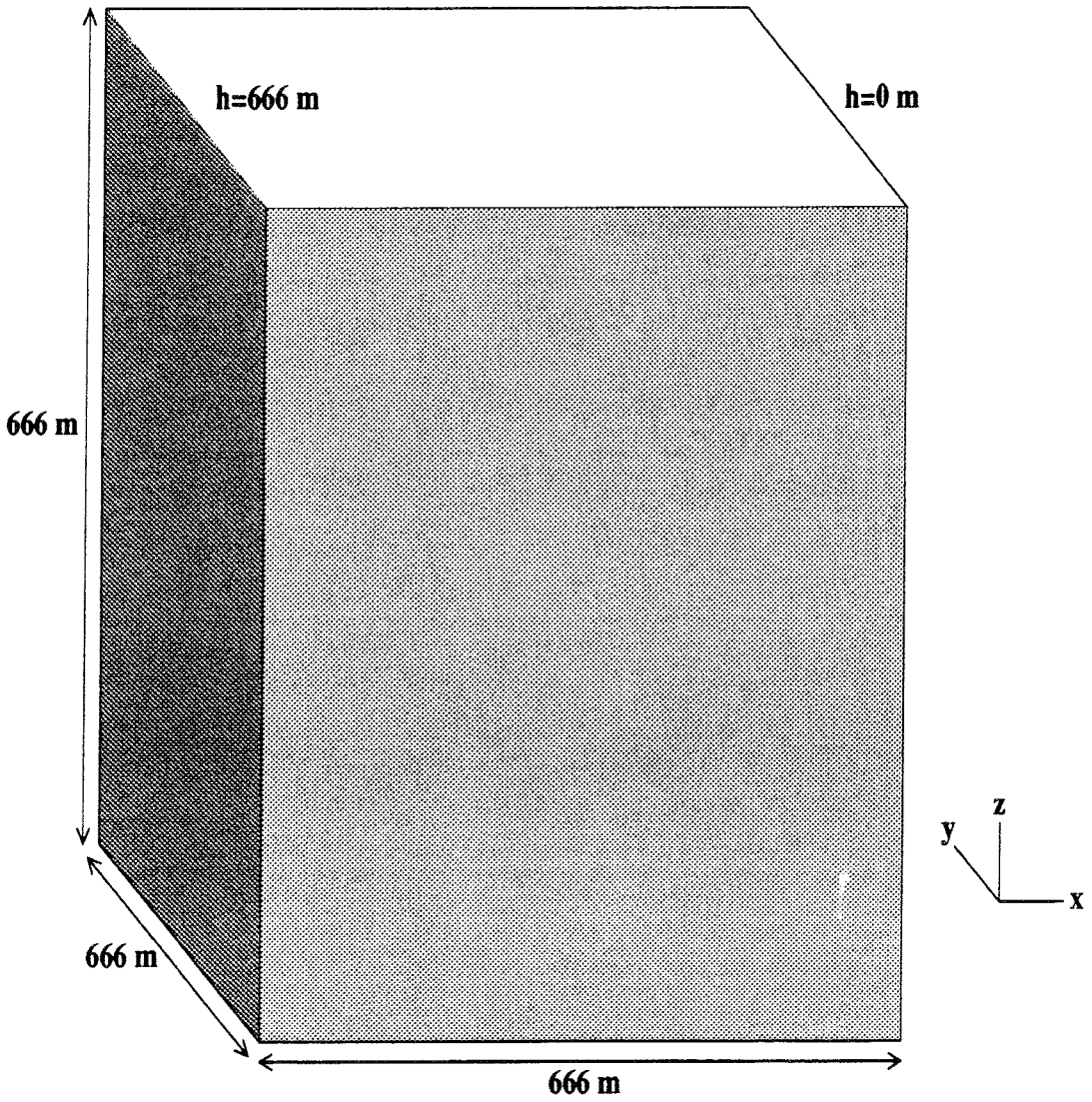

Figure 5.1: Domain and boundary conditions used for the three-dimensional calculations. h is the hydraulic head.

In this case, the grid used was fully three-dimensional, with a uniform head

gradient in the first direction, and no-flow boundaries in the other two directions. The number of grid points in the y and z directions was equal. Figure 5.1 shows the domain and boundary conditions used in the test case. The physical parameters used in the study are as shown in Table 5.1.

Grid dimensions	666m x 666m x 666m
Covariance model	exponential
Range parameter, λ	33.3m
Number of head nodes	41x41x41
Bandwidth factor	0.2
Number of sets of lines	4
Mean head gradient	1.0
Principal components of hydraulic conductivity	1.0, 1.0, 1.0
Porosity	0.1
Residual tolerance (used in HYDROGEOLOGY_EQ block)	1.0E-6
Tolerance (used in TRANSPORT block)	0.2

Table 5.1: Physical parameters used for the three-dimensional study at small variance.

The variance of the logarithm (to base 10) of the hydraulic conductivity was chosen to be 0.1886. This corresponds to a variance of 1.0 in natural logarithms. The analytical results of Dagan are expected to remain valid up to a variance of around 1.0, in natural logarithms. The HYDRASTAR input file used in this case is shown in Appendix C.

5.2 Transport Calculations

In the case of three-dimensional flow with isotropic hydraulic conductivity, Dagan's expressions for the variances of longitudinal and transverse displacement, X_{11}, X_{22} and X_{33} are

$$\frac{X_{11}}{\sigma^2\lambda^2} = 2t' - 2\left[\frac{8}{3} - \frac{4}{t'} + \frac{8}{t'^3} - \frac{8}{t'^2}\left(1 + \frac{1}{t'}\right)e^{-t'}\right], \tag{31}$$

$$\frac{X_{22}}{\sigma^2\lambda^2} = \frac{X_{33}}{\sigma^2\lambda^2} = 2\left[\frac{1}{3} - \frac{1}{t'} + \frac{4}{t'^3} - \left(\frac{4}{t'^3} + \frac{4}{t'^2} + \frac{1}{t'}\right)e^{-t'}\right]. \tag{32}$$

Figures 5.2, 5.3 and 5.4 show how the results calculated using HYDRASTAR compare with Dagan's analytic results, for both the longitudinal and transverse cases.

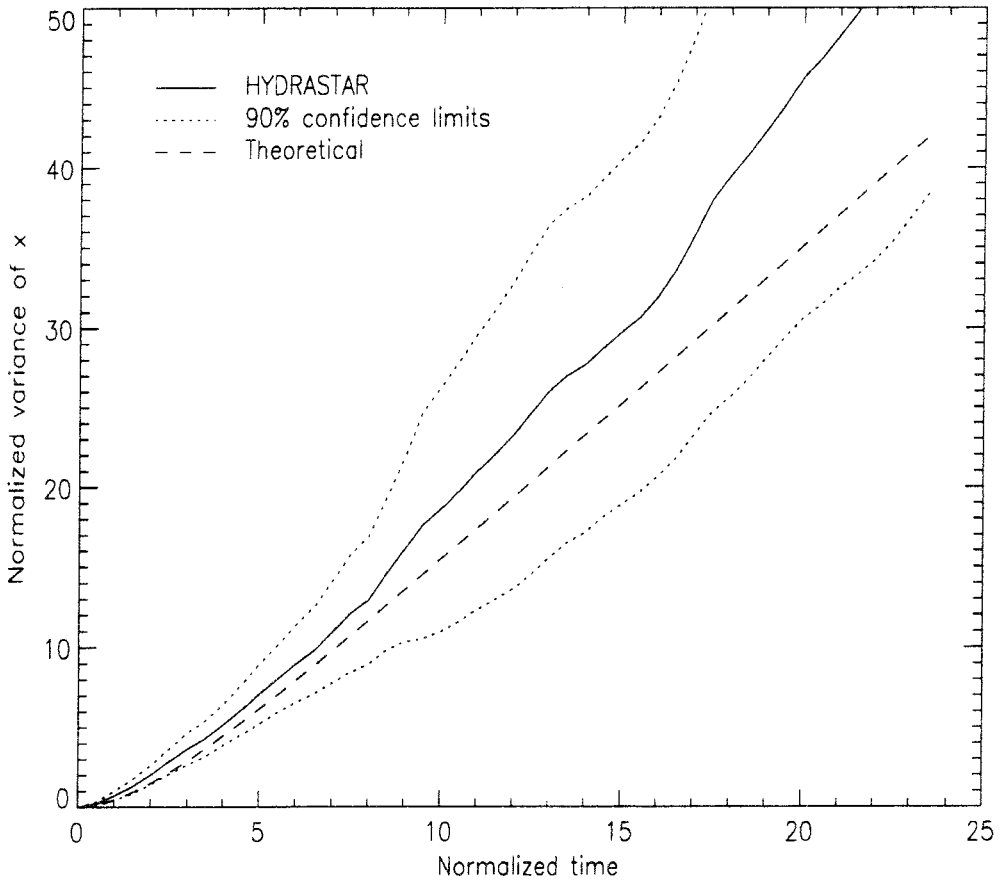

Figure 5.2: Plot of the normalized variance of the longitudinal displacement as a function of normalized time, for the case of three-dimensional flow and small variance of the logarithm of hydraulic conductivity. The 90% Guttman bounds and Dagan's analytical result are also plotted.

In this case the number of realizations was 100. As in the two-dimensional case, the calculated results are in good agreement with the analytic results, the analytic results being largely within the 90% confidence bounds.

Figures 5.5, 5.6 and 5.7 also show how the mean longitudinal and transverse displacements vary as a function of time. The time and the displacements are normalized with respect to the correlation length. As expected, the mean longitudinal displacement is proportional to time, with a mean speed approximately equal to the mean speed calculated by assuming that the effective hydraulic conductivity is equal to the prescribed mean hydraulic conductivity. The analytic result does lie outside the 90% confidence limits of the HYDRASTAR result, however. The mean displacements in the y and z directions are found to be approximately zero at all times, as expected.

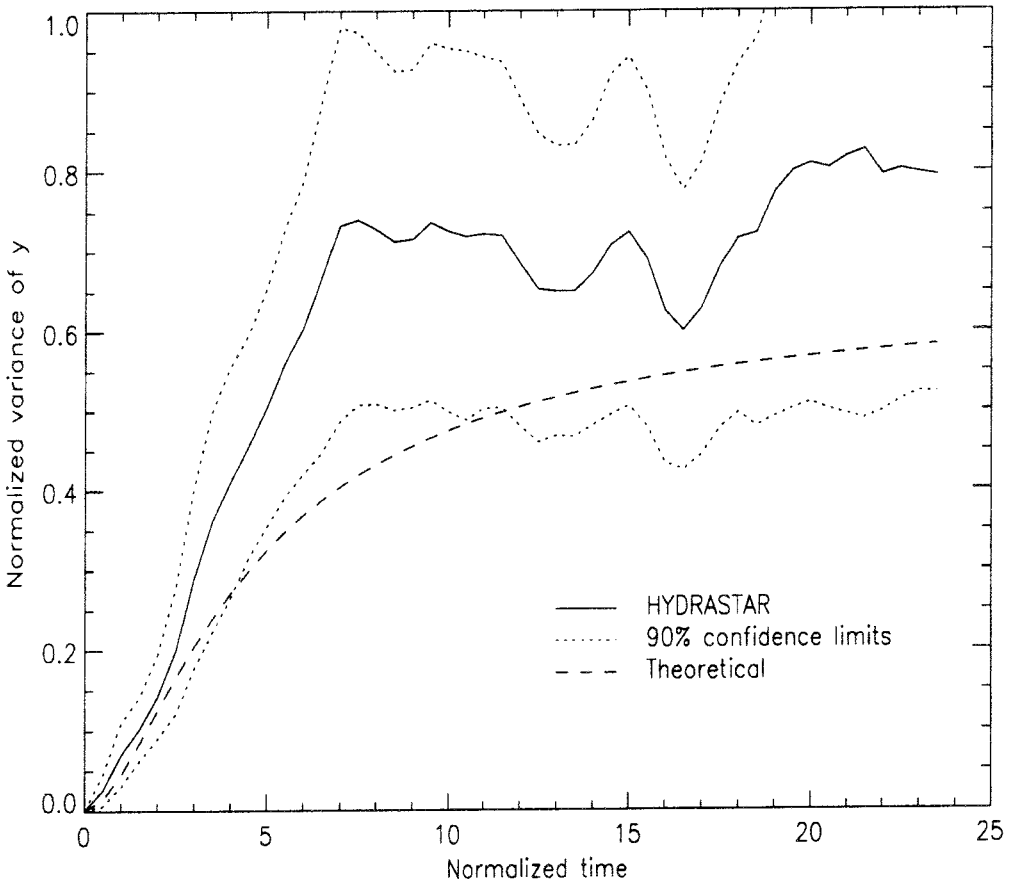

Figure 5.3: Plot of the normalized variance of the transverse displacement in the y direction as a function of normalized time, for the case of three-dimensional flow and small variance of the logarithm of hydraulic conductivity. The 90% Guttman bounds and Dagan's analytical result are also plotted.

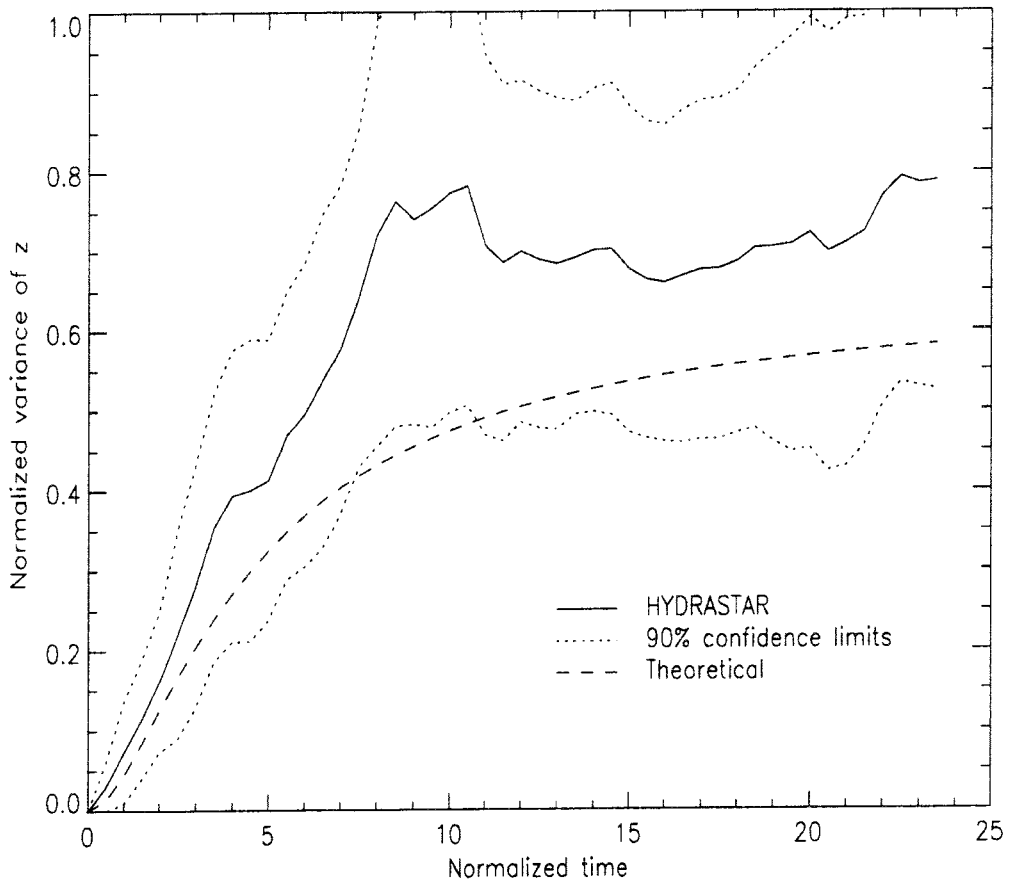

Figure 5.4: Plot of the normalized variance of the transverse displacement in the z direction as a function of normalized time, for the case of three-dimensional flow and small variance of the logarithm of hydraulic conductivity. The 90% Guttman bounds and Dagan's analytical result are also plotted.

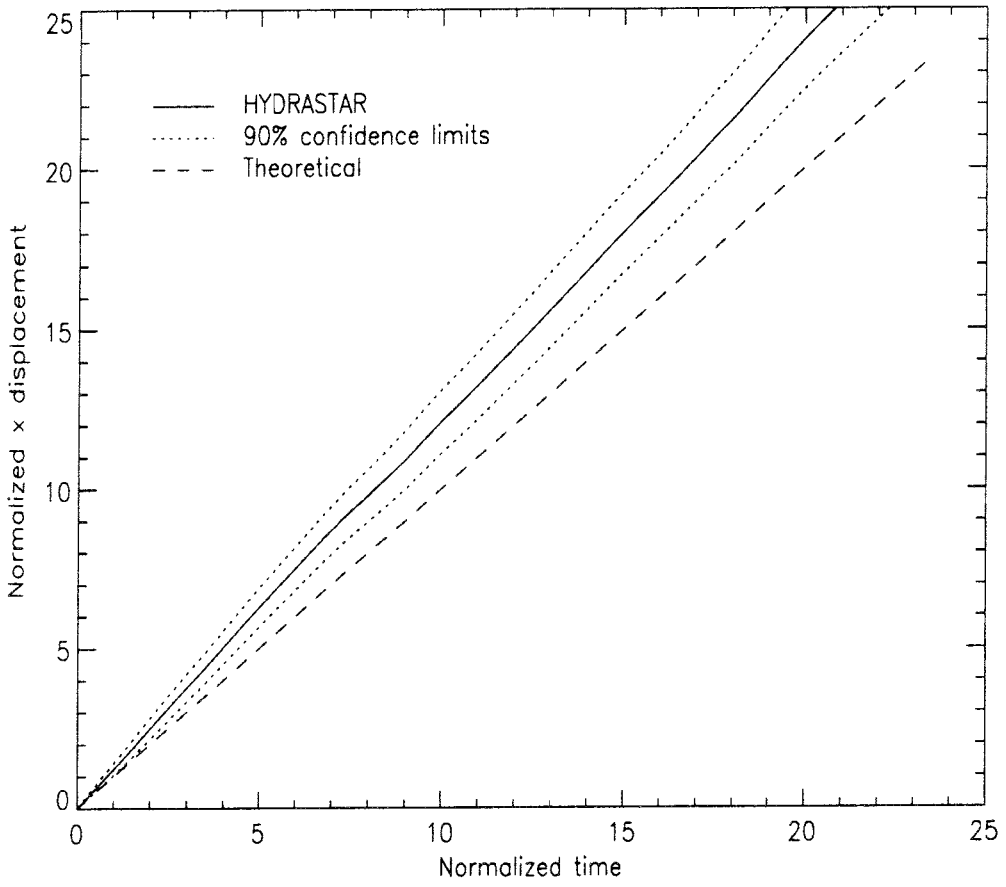

Figure 5.5: Plot of the normalized longitudinal displacement as a function of normalized time, for the case of three-dimensional flow and small variance of the logarithm of hydraulic conductivity. The 90% Guttman bounds are plotted and the theoretical result is also plotted for reference.

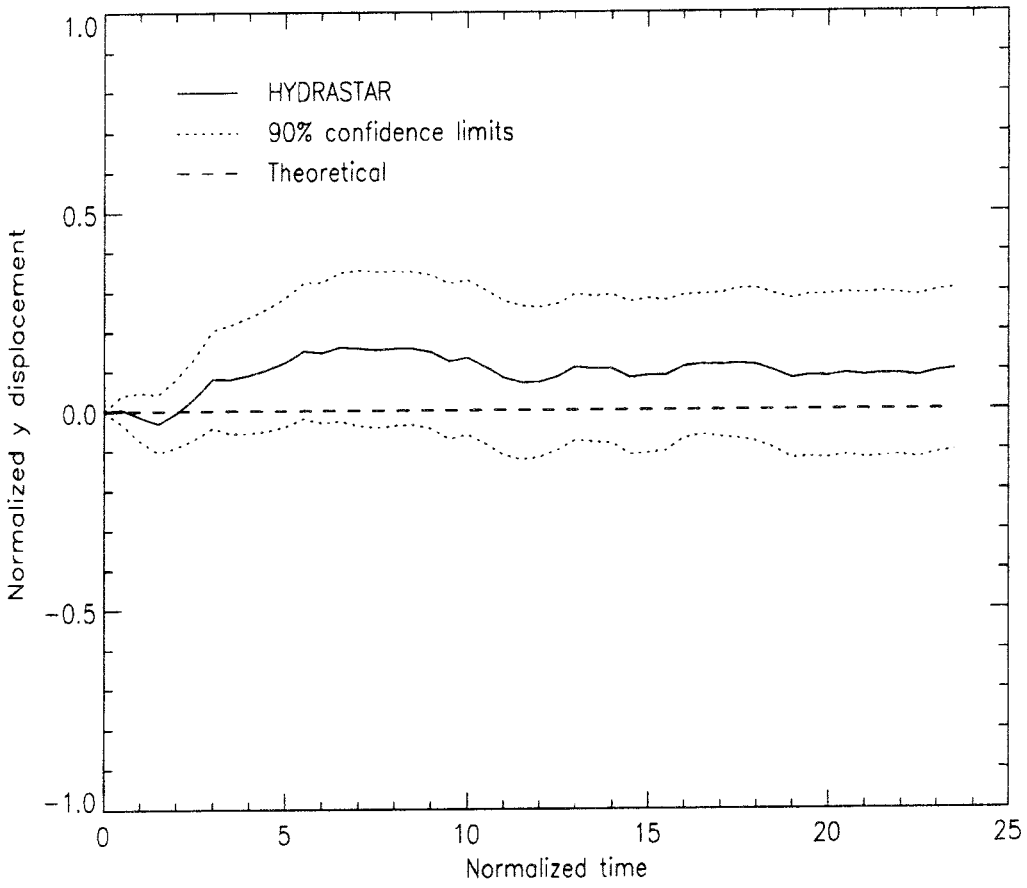

Figure 5.6: Plot of the normalized transverse displacement in the y direction as a function of normalized time, for the case of three-dimensional flow and small variance of the logarithm of hydraulic conductivity. The 90% Guttman bounds are plotted and the theoretical result is also plotted for reference.

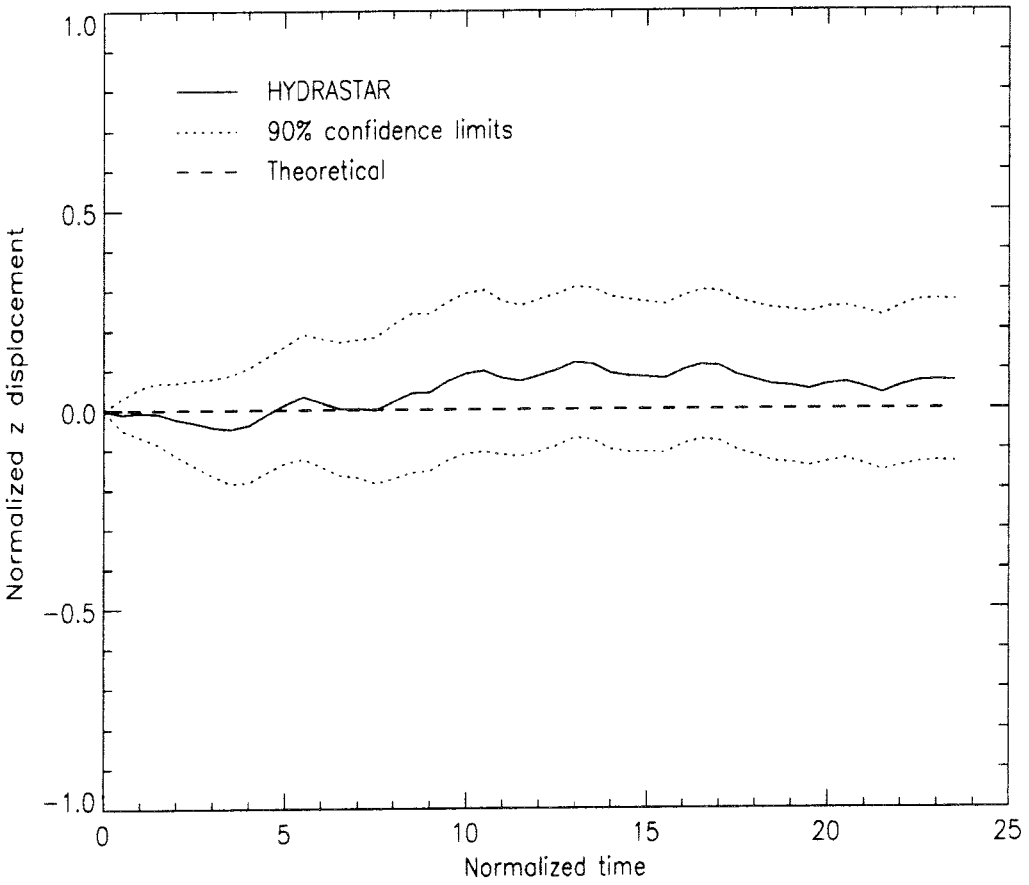

Figure 5.7: Plot of the normalized transverse displacement in the z direction as a function of normalized time, for the case of three-dimensional flow and small variance of the logarithm of hydraulic conductivity. The 90% Guttman bounds are plotted and the theoretical result is also plotted for reference.

5.3 Conclusions

The results calculated using HYDRASTAR using this test case are in good agreement with the results expected from theoretical considerations. In particular, the moments of particle displacement are in good agreement with those obtained by Dagan [7]. This indicates that HYDRASTAR is capable of calculating accurately both the flow and transport in three-dimensional flows with small variance of the logarithm of hydraulic conductivity.

6. ACKNOWLEDGMENT

This work was funded by SKB.

7. REFERENCES

1. S. Norman. HYDRASTAR- A Code for Stochastic Simulation of Groundwater Flow. SKB Technical Report TR 92-12, 1992.

2. User's guide to HYDRASTAR 1.4. SKB Report AR 94-14, 1994.

3. S. Norman. Verification of HYDRASTAR - A code for stochastic continuum simulation of groundwater flow. SKB Technical Report TR 91-27, 1991.

4. The International HYDROCOIN Project: Groundwater hydrology modelling strategies for performance assessment of nuclear waste disposal. Level 1: Code verification. OECD, 1983.

5. R. Ababou A. F. B. Thompson and L. W. Gelhar. Implementation of the three-dimensional turning bands random field generator. *Water Resour. Res.*, 25(10):2227–2243, 1989.

6. A. L. Gutjahr. Fast Fourier transforms for random field generation. New Mexico Tech. Technical Report, 1992.

7. G. Dagan. *Flow and Transport in Porous Formations.* Springer-Verlag, 1989.

8. A. G. Journel and C. Huijbregts. *Mining Geostatistics.* Academic Press, 1978.

9. A. Montoglou and J. L. Wilson. The Turning Bands method for simulation of random fields using line generation by a spectral method. *Water Resour. Res.*, 18(5):1379–1394, 1982.

10. Y. Rubin. Stochastic modelling of macrodispersion in heterogeneous porous media. *Water Resour. Res.*, 26(1):133–141, 1990.

11. L. J. Hartley and S. T. Morris. Spatial variability test case 1: Uniform average flow in a single medium in two dimensions. Nirex NSS Report, in preparation, 1994.

12. Y. Rubin. Confidence bounds on risk assessments for underground nuclear waste repositories. *Terra Nova*, 1:79–83, 1989.

13. L. J. Hartley and K. A. Cliffe. SPV2D (Release 1.0) User Guide. AEA Report AEA-D&W-0738, in preparation, 1994.

14. M. Hill. Finite-element calculation of groundwater flow through fractal porous media. MSc Disseration, University of Bristol, 1993.

APPENDIX A

Input dataset for Section 3

This Appendix lists the HYDRASTAR input file used for the calculation described in Section 3. The format of the input is described in the HYDRASTAR User Guide [2]. This case was run using version 1.4.17 of HYDRASTAR.

```
#
SYSTEM IGNORE_ERRORS
##
BEGIN_BLOCK COVARIANCE
        VARIANCE        0.1886
        RANGE           -33.3
        BEGIN_DEF ANISOTROPY
                KXX     1.0
                KXY     0.0
                KXZ     0.0
                KYY     1.0
                KYZ     0.0
                KZZ     1.0
        END_DEF
        RELATIVE_TOL    0.0
        NUM_ICOSAHEDRON 4
        NUM_LINES       0
        ORIGIN          0.0 0.0 0.0
        MUL_FACTOR      100.0
        TRUNCATION      1.0E6
END_BLOCK
###
BEGIN_BLOCK GEOM
        AXISLENGTH      1000.0 1000.0 0.1
        NUMBER_OF_NODES 121  121  4
        BOUNDARY        SIMPLE
        GRADIENT        -1.0 0.0  0.0
        LEVEL           1000.0
        NOFLOW_SIDES
           YTOP
           YBOT
           ZTOP
           ZBOT
END_SIDES
END_BLOCK
##
##
```

```
BEGIN_BLOCK KRGE_NBH
END_BLOCK
##
##
BEGIN_BLOCK KRIGE

END_BLOCK
##
BEGIN_BLOCK HYDROLOGY_EQ
        NUM_ITERATIONS    30000
        RESIDUAL_TOL      1.00E-6
        PRECOND           DIAGONAL
END_BLOCK
#
#
#
BEGIN_BLOCK TRANSPORT
        TRANSPORT_MODEL STREAM
        PLOT_TIMES      1
        TRACERS
       100.0  500.0  0.05 1
        END_LIST
        BACK_INTERPOL   BACKINT
        INTERVALS       AUTOMATIC
COLOURS          2
        LOGON
        TOLERANCE       0.2
        PRESENTATION    0.1
        CELL_SHIFTS     300
        PLOTTING_MOMENTS        1.E1
        STREAM_TUBES    1
        DIVISION        SPATIAL
        VIEW            ALL
END_BLOCK
##
#
BEGIN_BLOCK RESULT_ESTIMATION
        PERIOD  1
        SAVE_TRANSPORT  NOTRANSPORT


BEGIN_DEF POINT
NAME V1
RESULT_TYPE VELOCITY1
PROBABILITY 1.0
          BEGIN_DEF SLICE
          NORMAL 0.0 0.0 1.0
```

```
          LENGTH 0.0
         WIDTH 0.1
          END_DEF
END_DEF

BEGIN_DEF POINT
NAME V2
RESULT_TYPE VELOCITY2
PROBABILITY 1.0
          BEGIN_DEF SLICE
          NORMAL 0.0 0.0 1.0
          LENGTH 0.0
         WIDTH 0.1
          END_DEF
END_DEF

BEGIN_DEF LAGCLASS
NAME V2
RESULT_TYPE VELOCITY2
PROBABILITY 1.0
POLAR_VECTOR 1.0 0.0 0.0
R_DELIMITERS PREDETERMINED
RADIAL
33.0
67.0
100.0
133.0
167.0
200.0
233.0
267.0
300.0
END_LIST
ANGULAR
10.0
80.0
90.0
END_LIST
END_DEF

  BEGIN_DEF VARIOGRAM
  NAME V2
  POINT V2
  LAGCLASS V2
  END_DEF

BEGIN_DEF EXPECTATION
```

```
NAME V1
POINT V1
END_DEF

BEGIN_DEF EXPECTATION
NAME V2
POINT V2
END_DEF

END_BLOCK
```

APPENDIX B

Input dataset for Section 4

This Appendix lists the HYDRASTAR input file used for the calculation described in Section 4. The format of the input is described in the HYDRASTAR User Guide [2]. This case was run using version 1.4.11 of HYDRASTAR.

```
#
SYSTEM IGNORE_ERRORS
##
BEGIN_BLOCK COVARIANCE
        VARIANCE        0.943
        RANGE           -33.3
        BEGIN_DEF ANISOTROPY
                KXX     1.0
                KXY     0.0
                KXZ     0.0
                KYY     1.0
                KYZ     0.0
                KZZ     1.0
        END_DEF
        RELATIVE_TOL    0.0
        NUM_ICOSAHEDRON 4
        NUM_LINES       0
        ORIGIN          0.0 0.0 0.0
        MUL_FACTOR      25.0
        TRUNCATION      1.0E6
END_BLOCK
###
BEGIN_BLOCK GEOM
        AXISLENGTH      1332.0 832.5 0.1
        NUMBER_OF_NODES 321  201  4
        BOUNDARY        SIMPLE
        GRADIENT        -1.0 0.0  0.0
        LEVEL           1332.0
        NOFLOW_SIDES
           YTOP
           YBOT
           ZTOP
           ZBOT
END_SIDES
END_BLOCK
##
##
```

```
BEGIN_BLOCK KRGE_NBH
END_BLOCK
##
##
BEGIN_BLOCK KRIGE

END_BLOCK
##
BEGIN_BLOCK HYDROLOGY_EQ
        NUM_ITERATIONS     40000
        RESIDUAL_TOL       1.00E-6
        PRECOND            DIAGONAL
END_BLOCK
#
#
#
BEGIN_BLOCK TRANSPORT
        TRANSPORT_MODEL STREAM
        PLOT_TIMES      1
        TRACERS
       50.0  416.25  0.05 1
        END_LIST
        BACK_INTERPOL   BACKINT
        INTERVALS       AUTOMATIC
COLOURS          2
        LOGON
        TOLERANCE       0.2
        PRESENTATION    0.1
        CELL_SHIFTS     1000
        PLOTTING_MOMENTS        1.E1
        STREAM_TUBES    1
        DIVISION        SPATIAL
        VIEW            ALL
END_BLOCK
```

APPENDIX C

Input dataset for Section 5

This Appendix lists the HYDRASTAR input file used for the calculation described in Section 5. The format of the input is described in the HYDRASTAR User Guide [2]. This case was run using version 1.4.17 of HYDRASTAR.

```
#
SYSTEM IGNORE_ERRORS
##
BEGIN_BLOCK COVARIANCE
        VARIANCE        0.1886
        RANGE           -33.3
        BEGIN_DEF ANISOTROPY
                KXX     1.0
                KXY     0.0
                KXZ     0.0
                KYY     1.0
                KYZ     0.0
                KZZ     1.0
        END_DEF
        RELATIVE_TOL    0.0
        NUM_ICOSAHEDRON 4
        NUM_LINES       0
        ORIGIN          0.0 0.0 0.0
        MUL_FACTOR      0.2
        TRUNCATION      1.0E6
END_BLOCK
###
BEGIN_BLOCK GEOM
        AXISLENGTH      1665.0 532.8 532.8
        NUMBER_OF_NODES 201 65 65
        BOUNDARY        SIMPLE
        GRADIENT        -1.0 0.0  0.0
        LEVEL           1665.0
        NOFLOW_SIDES
           YTOP
           YBOT
           ZTOP
           ZBOT
END_SIDES
END_BLOCK
##
##
```

```
BEGIN_BLOCK KRGE_NBH
END_BLOCK
##
##
BEGIN_BLOCK KRIGE

END_BLOCK
##
BEGIN_BLOCK HYDROLOGY_EQ
        NUM_ITERATIONS    10000
        RESIDUAL_TOL      1.00E-6
        PRECOND           DIAGONAL
END_BLOCK
#
#
#
BEGIN_BLOCK TRANSPORT
        TRANSPORT_MODEL STREAM
        PLOT_TIMES      1
        TRACERS
       33.3 266.4 266.4 1
        END_LIST
        BACK_INTERPOL   BACKINT
        INTERVALS       AUTOMATIC
COLOURS          2
        LOGON
        TOLERANCE       0.2
        PRESENTATION    0.1
        CELL_SHIFTS     1200
        PLOTTING_MOMENTS        1.E1
        STREAM_TUBES    1
        DIVISION        SPATIAL
        VIEW            ALL
END_BLOCK
##
```

List of SKB reports

Annual Reports

1977-78
TR 121
KBS Technical Reports 1 – 120
Summaries
Stockholm, May 1979

1979
TR 79-28
The KBS Annual Report 1979
KBS Technical Reports 79-01 – 79-27
Summaries
Stockholm, March 1980

1980
TR 80-26
The KBS Annual Report 1980
KBS Technical Reports 80-01 – 80-25
Summaries
Stockholm, March 1981

1981
TR 81-17
The KBS Annual Report 1981
KBS Technical Reports 81-01 – 81-16
Summaries
Stockholm, April 1982

1982
TR 82-28
The KBS Annual Report 1982
KBS Technical Reports 82-01 – 82-27
Summaries
Stockholm, July 1983

1983
TR 83-77
The KBS Annual Report 1983
KBS Technical Reports 83-01 – 83-76
Summaries
Stockholm, June 1984

1984
TR 85-01
Annual Research and Development Report 1984
Including Summaries of Technical Reports Issued during 1984. (Technical Reports 84-01 – 84-19)
Stockholm, June 1985

1985
TR 85-20
Annual Research and Development Report 1985
Including Summaries of Technical Reports Issued during 1985. (Technical Reports 85-01 – 85-19)
Stockholm, May 1986

1986
TR 86-31
SKB Annual Report 1986
Including Summaries of Technical Reports Issued during 1986
Stockholm, May 1987

1987
TR 87-33
SKB Annual Report 1987
Including Summaries of Technical Reports Issued during 1987
Stockholm, May 1988

1988
TR 88-32
SKB Annual Report 1988
Including Summaries of Technical Reports Issued during 1988
Stockholm, May 1989

1989
TR 89-40
SKB Annual Report 1989
Including Summaries of Technical Reports Issued during 1989
Stockholm, May 1990

1990
TR 90-46
SKB Annual Report 1990
Including Summaries of Technical Reports Issued during 1990
Stockholm, May 1991

1991
TR 91-64
SKB Annual Report 1991
Including Summaries of Technical Reports Issued during 1991
Stockholm, April 1992

1992
TR 92-46
SKB Annual Report 1992
Including Summaries of Technical Reports Issued during 1992
Stockholm, May 1993

Technical Reports
List of SKB Technical Reports 1994

TR 94-01
Anaerobic oxidation of carbon steel in granitic groundwaters: A review of the relevant literature
N Platts, D J Blackwood, C C Naish
AEA Technology, UK
February 1994

TR 94-02
Time evolution of dissolved oxygen and redox conditions in a HLW repository
Paul Wersin, Kastriot Spahiu, Jordi Bruno
MBT Technología Ambiental, Cerdanyola, Spain
February 1994

TR 94-03
Reassessment of seismic reflection data from the Finnsjön study site and prospectives for future surveys
Calin Cosma[1], Christopher Juhlin[2], Olle Olsson[3]
[1] Vibrometric Oy, Helsinki, Finland
[2] Section for Solid Earth Physics, Department of Geophysics, Uppsala University, Sweden
[3] Conterra AB, Uppsala, Sweden
February 1994

TR 94-04
Final report of the AECL/SKB Cigar Lake Analog Study
Jan Cramer (ed.)[1], John Smellie (ed.)[2]
[1] AECL, Canada
[2] Conterra AB, Uppsala, Sweden
May 1994

TR 94-05
Tectonic regimes in the Baltic Shield during the last 1200 Ma - A review
Sven Åke Larsson[1,2], Eva-Lena Tullborg[2]
[1] Department of Geology, Chalmers University of Technology/Göteborg University
[2] Terralogica AB
November 1993

TR 94-06
First workshop on design and construction of deep repositories - Theme: Excavation through water-conducting major fracture zones Såstaholm Sweden, March 30-31 1993
Göran Bäckblom (ed.), Christer Svemar (ed.)
Swedish Nuclear Fuel & Waste Management Co, SKB
January 1994

TR 94-07
INTRAVAL Working Group 2 summary report on Phase 2 analysis of the Finnsjön test case
Peter Andersson (ed.)[1], Anders Winberg (ed.)[2]
[1] GEOSIGMA, Uppsala, Sweden
[2] Conterra, Göteborg, Sweden
January 1994

TR 94-08
The structure of conceptual models with application to the Äspö HRL Project
Olle Olsson[1], Göran Bäckblom[2], Gunnar Gustafson[3], Ingvar Rhén[4], Roy Stanfors[5], Peter Wikberg[2]
1 Conterra AB
2 SKB
3 CTH
4 VBB/VIAK
5 RS Consulting
May 1994

TR 94-09
Tectonic framework of the Hanö Bay area, southern Baltic Sea
Kjell O Wannäs, Tom Flodén
Institutionen för geologi och geokemi, Stockholms universitet
June 1994

TR 94-10
Project Caesium–An ion exchange model for the prediction of distribution coefficients of caesium in bentonite
Hans Wanner[1], Yngve Albinsson[2], Erich Wieland[1]
[1] MBT Umwelttechnik AG, Zürich, Switzerland
[2] Chalmers University of Technology, Gothenburg, Sweden
June 1994

TR 94-11
Äspö Hard Rock Laboratory Annual Report 1993
SKB
June 1994

TR 94-12
Research on corrosion aspects of the Advanced Cold Process Canister
D J Blackwood, A R Hoch, C C Naish, A Rance, S M Sharland
AEA Technology, Harwell Laboratory, UK
January 1994

TR 94-13
Assessment study of the stresses induced by corrosion in the Advanced Cold Process Canister
A R Hoch, S M Sharland
Chemical Studies Department, Radwaste Disposal Division, AEA Decommissioning and Radwaste, Harwell Laboratory, UK
October 1993

TR 94-14
Performance of the SKB Copper/Steel Canister
Hans Widén[1], Patrik Sellin[2]
[1] Kemakta Konsult AB, Stockholm, Sweden
[2] Svensk Kärnbränslehantering AB, Stockholm, Sweden
September 1994

TR 94-15
Modelling of nitric acid production in the Advanced Cold Process Canister due to irradiation of moist air
J Henshaw
AEA Technology, Decommissioning & Waste Management/Reactor Services, Harwell, UK
January 1994

TR 94-16
Kinetic and thermodynamic studies of uranium minerals. Assessment of the long-term evolution of spent nuclear fuel
Ignasi Casas[1], Jordi Bruno[1], Esther Cera[1], Robert J Finch[2], Rodney C Ewing[2]
[1] MBT Tecnología Ambiental, Cerdanyola, Spain
[2] Department of Earth and Planetary Sciences, University of New Mexico, Albuquerque, NM, USA
October 1994

TR 94-17
Summary report of the experiences from TVO's site investigations
Antti Öhberg[1], Pauli Saksa[2], Henry Ahokas[2], Paula Ruotsalainen[2], Margit Snellman[3]
[1] Saanio & Riekkola Consulting Engineers, Helsinki, Finland
[2] Fintact Ky, Helsinki, Finland
[3] Imatran Voima Oy, Helsinki, Finland
May 1994

TR 94-18
AECL strategy for surface-based investigations of potential disposal sites and the development of a geosphere model for a site
S H Whitaker, A Brown, C C Davison, M Gascoyne, G S Lodha, D R Stevenson, G A Thorne, D Tomsons
AECL Research, Whiteshell Laboratories, Pinawa, Manitoba, Canada
May 1994

TR 94-19
Deep drilling KLX 02. Drilling and documentation of a 1700 m deep borehole at Laxemar, Sweden
O Andersson
VBB VIAK AB, Malmö
August 1994

TR 94-20
Technology and costs for decommissioning the Swedish nuclear power plants
Swedish Nuclear Fuel and Waste Management Co, Stockholm, Sweden
June 1994